Integer-spin electron paramagnetic resonance of iron proteins

Michael P. Hendrich* and Peter G. Debrunner‡
*Gray Freshwater Biological Institute, University of Minnesota, Navarre, Minnesota 55392; and ‡Department of Physics, University of Illinois at Urbana-Champaign, Urbana, Illinois 61801

ABSTRACT A quantitative interpretation is presented for EPR spectra from integer-spin metal centers having large zero-field splittings. Integer-spin, or non-Kramers, centers are common in metalloproteins and many give EPR signals, but a quantitative understanding has been lacking until now. Heterogeneity of the metal's local environment will result in a significant spread in zero-field splittings and in broadened EPR signals. Using the spin Hamiltonian $\mathcal{H}_s = \mathbf{S} \cdot \mathbf{D} \cdot \mathbf{S} + \beta \mathbf{S} \cdot \mathbf{g} \cdot \mathbf{B}$ and some simple assumptions about the nature of the zero-field parameter distributions, a lineshape model was devised which allows accurate simulation of single crystal and frozen solution spectra. The model was tested on single crystals of magnetically dilute ferrous fluosilicate. Data and analyses from proteins and active-site models are presented with the microwave field $\mathbf{B}_1$ either parallel or perpendicular to $\mathbf{B}$. Quantitative agreement of observed and predicted signal intensities is found for the two $\mathbf{B}_1$ orientations. Methods of spin quantitation are given and are shown to predict an unknown concentration relative to a standard with known concentration. The fact that the standard may be either a non-Kramers or a Kramers center is further proof of the model's validity. The magnitude of the splitting in zero magnetic field is of critical importance; it affects not only the chance of signal observation, but also the quantitation accuracy. Experiments taken at microwave frequencies of 9 and 35 GHz demonstrate the need for high-frequency data as only a fraction of the molecules give signals at 9 GHz.

INTRODUCTION

In recent years, a number of novel electron paramagnetic resonance (EPR) signals from iron proteins with integer spin have been reported in the literature. Integer-spin resonances have been observed from the mononuclear ferrous sites of myoglobin (Mb) (1) and transferrin (2), the two-iron sites of hemerythrin azide (3), methane monooxygenase (4), the three-iron sites of reduced ferredoxin II (5, 6) and aconitase (Hendrich, M., unpublished result), and the iron-copper sites of cytochrome *c* oxidases from beef heart (2, 7, 8) and yeast (9). In previous work we have presented EPR data on mononuclear ferrous complexes (10), and in this paper we give a detailed interpretation of integer-spin EPR spectra and discuss methods of spin quantitation. We also present unpublished spectra of several of the proteins mentioned above.

EPR spectra can be assigned to one of two classes depending on the number of unpaired electrons involved. The first class, comprised of spin centers having an odd number of electrons and thus half-integer spin, is referred to as Kramers centers. As a result of the time reversal invariance of the electrostatic Hamiltonian, i.e., in the absence of magnetic interactions, Kramers' theorem states that a center with an odd number of electrons must have at least doubly degenerate spin states. The time-conjugate, degenerate spin states are referred to as Kramers doublets. An external magnetic field removes the time reversal invariance and splits the Kramers doublets linearly with field strength B by an energy $\delta\epsilon = g\beta B$, and the resonance condition $\delta\epsilon = h\nu$ becomes

$$\delta\epsilon = h\nu = g\beta B \qquad (1)$$

For an X band spectrometer ($h\nu \approx 0.3\text{cm}^{-1}$), the resonance condition (Eq. 1) is satisfied for $g = 2$ with $B \approx 300$ mT.

The second class of EPR spectra arises from paramagnetic centers having an even number of unpaired electrons and thus integer spin; they are referred to as non-Kramers centers. This class can be further divided into two subclasses. (*a*) Biradical organic triplets and metal centers with fine structure energies small relative to the Zeeman interaction. This subclass can be treated with methods applicable to half-integer spin centers (11) and shall not be discussed further. (*b*) Metal centers with fine structure energies large relative to the Zeeman interaction. We will focus on the latter subclass and refer to the observed spectra as "integer-spin EPR signals." Of interest in this work are integer-spin signals that are generated by microwave transitions between a pair of levels in a spin multiplet with a splitting Δ in zero field that satisfies the condition $\Delta < h\nu$. Because the pair of levels is not degenerate in zero field, a magnetic field will increase the

0006-3495/89/09/489/18 $2.00

splitting of the levels quadratically. As we shall see in the theory section, the resonance condition for such non-Kramers doublets is

$$(h\nu)^2 = (\tilde{g}\beta B)^2 + \Delta^2, \quad (2)$$

where $\tilde{g}$ is an angle-dependent effective g-value. Thus the lineshape of non-Kramers spectra is expected to differ markedly from spectra of Kramers systems, where the doublets split linearly with magnetic field.

The biologically important transition metals V, Mn, Fe, Co, Ni, Mo occur in even and odd valence states and may, in particular, assume spin $S = 1$ or $S = 2$. The same spin states are also known to occur in some exchange-coupled metal clusters. Integer-spin EPR of metalloproteins, however, has not been fully exploited for a number of reasons. (*a*) Observation of resonance in non-Kramers doublets depends critically on the condition $h\nu > \Delta$, which may not be satisfied in many cases of interest with commonly available EPR frequencies (9 and 35 GHz). (*b*) Signals are generally observable near helium temperatures only because of rapid spin relaxation rates. (*c*) The resonances are generally quite broad due to random orientation of the molecules and due to a spread in the parameter Δ. As a consequence, the signals are small and hard to detect even if the spin concentration is high. (*d*) Computer simulations are needed to interpret the spectra and to quantitate the number of spins as there is no simple, intuitive relation between g-values and lineshapes. (*e*) Few previous studies exist with which to compare new data.

We have had some success in understanding integer-spin EPR spectra from iron complexes, thus we will concentrate on iron species. We have shown that EPR signals of myoglobin (Mb) can be observed from difference measurements of diamagnetic MbCO and its photoproduct Mb*(CO) (10). Previous work in the field, for the most part, has dealt with well-defined single crystals, e.g., FeF_2 (12) and ferrous fluosilicate (FFS) (13, 14). We have verified our simulation routine on magnetically dilute single crystals of FFS and will briefly discuss the results. In addition, we will present work on frozen solutions of aqueous iron(II), iron(II) proteins, and active-site models.

MATERIALS AND METHODS

Sample preparation

Iron doped zinc fluosilicate crystals were grown from a solution containing 31.9% hydrofluosilicic acid in H_2O (H_2SiF_6, Baker Chemical Co., Phillipsburg, NJ) and a saturating amount of the proper ratio of zinc (Fred Portz Jr. Associates, Waukasha, WI) to iron (Mallinckrodt Inc., St. Louis, MO; 95% assay) metal. The metal was added to the acid until no reaction was observed, followed by filtering off the excess metal. The solution was placed in a lightly capped bottle and crystals were available a few days later. The crystals were mounted on quartz flats and aligned visually under a microscope; a small amount of the mother liquor held the crystal in place. The mounted crystal was promptly frozen in liquid nitrogen. An atomic absorption measurement on a crystal of what will be referred to as 4% iron doped zinc fluosilicate found an iron atomic percentage of 3.7.

Magnetically dilute solutions of hexaquo ferrous ions were prepared by dissolving an appropriate amount of either $FeSO_4 \cdot 7H_2O$ (Mallinckrodt Inc.) or $FeCl_2 \cdot 4H_2O$ (Fisher Scientific Co., Pittsburgh, PA) into doubly distilled water. Several identical samples were reduced with $Na_2S_2O_4$ (Fisher Scientific Co.), and iron concentrations were determined by plasma emission spectroscopy. Aqueous solutions of magnetically dilute ferrous ethylenediamine tetraacetate (FeEDTA) were prepared under argon atmosphere with Na_2 EDTA (Sigma Chemical Co., St. Louis, MO; 99% assay) and $FeSO_4 \cdot 7H_2O$. All solutions were frozen and stored in liquid nitrogen shortly after preparation.

Stock solutions of sperm whale metMb (whale skeletal muscle tissue, type II; Sigma Chemical Co.) were prepared in 50 mM KP_i buffer, pH = 6.85. DeoxyMb was prepared by exchanging the gas over a metMb solution with argon followed by reduction with a small amount of $Na_2S_2O_4$. CarbonmonoxyMb (MbCO) was prepared similarly except the exchange gas was CO. An optical spectrum of the MbCO sample verified CO binding. OxyMb was prepared by exposing a deoxyMb sample to oxygen. The solutions were frozen, stored in liquid nitrogen, and kept in the dark until measurements were made. Control samples of deoxygenated and CO-exchanged buffer containing no Mb were prepared in a similar fashion.

The model heme complex Fe(II) 2-methylimidazole meso-tetraphenylporphyrin (FeTPP) (15) was a gift from Prof. Christopher Reed (University of Southern California). FeTPP crystals were sealed in an EPR sample tube with wax under a nitrogen atmosphere. Two similar model heme compounds, Fe(II) imidazole protoporphyrin IX CO and Fe(II) 2-methylimidazole protoporphyrin IX CO, were prepared in an aqueous, 50% glycerol solution (16) employing the methods of the MbCO preparation.

The yeast (17) and beef heart cytochrome *c* oxidases were gifts from Dr. Hsin Wang (California Institute of Technology). The azide complex of hemerythrin was a gift from Prof. Donald Kurtz (University of Georgia).

A number of the solution samples were prepared in glycerol (Fisher Scientific Co.; 99% assay); the glycerol was added to the solution before the reduction or deaeration step.

Instrumental

X band (9 GHz) EPR measurements were performed on an ER 200D spectrometer (Bruker Instruments, Inc., Billerica, MA) using a liquid helium flow cryostat (Oxford Instruments, Oxford, UK). Spectra were digitally recorded on an ASPECT 2000 computer. When recording spectra for purpose of comparison with simulation, all instrumental parameters (microwave power, field modulation, sweep rate, etc.) were appropriately varied to avoid instrumental artifacts. The spectra reported were generally recorded in a nonsaturating microwave power regime, i.e., we verified in each case the proportionality: signal intensity ~ (microwave power)$^{1/2}$.

The microwave frequency was measured with a model 6245A frequency counter (Systron Donner, Concord, CA) and the DC magnetic field was calibrated with an ER 035 NMR gaussmeter (Bruker Instruments, Inc.). The gaussmeter is not sensitive to magnetic fields <80 mT. At a field of <5–10 mT, the field regulation does not function, causing an anomaly in the EPR spectrum.

A model E-236 bimodal cavity (Varian Associates, Inc., Palo Alto, CA) was used to generate the microwave magnetic fields $\mathbf{B}_1 \parallel \mathbf{B}$ and $\mathbf{B}_1 \perp \mathbf{B}$. The frequencies of the two modes of the cavity occasionally coincide when the cavity is loaded with the quartz cryostat and sample tube. To separate the modes (2), two quartz rods (1-mm diameter) were mounted on a quartz tube and placed in the cavity via the illumination port. The electric field at the quartz rods is greater in the $\mathbf{B}_1 \perp \mathbf{B}$ mode, causing a decrease in frequency of the perpendicular mode. The resulting frequency separation was typically 50 MHz and no appreciable mode overlap occurred. The magnitude of $\mathbf{B}_1$ at cavity center was measured using the method of perturbing spheres (18, 18a) with the cryostat and sample tube in place; $\mathbf{B}_1$ was found to be 0.037 mT ($\mathbf{B}_1 \parallel \mathbf{B}$) or 0.055 mT ($\mathbf{B}_1 \perp \mathbf{B}$) at a nominal incident power of 200 mW.

The sample temperature, where needed, was determined relative to the known temperature dependence of the EPR signal of metMb ($D = 9.5$ cm^{-1} (19)) and one known temperature point. MetMb was either an impurity or purposely introduced by freezing a capillary containing metMb into the sample.

A light path to the sample was available while the mode separation rods were in place. The photolysis product Mb*(CO) was prepared by illumination in situ at 4 K for 30 min, and the time course of the EPR signals could be monitored during photolysis. The particular light source (typically 600-W xenon or 150-W tungsten lamp) was found not to be critical; one would like maximal intensity in the range 450–600 nm.

Q band (35 GHz) EPR experiments were performed on a Century-line spectrometer (Varian Associates, Inc.) using a Heli-Tran liquid helium flow cryostat (Air Products & Chemicals, Inc., Allentown, PA) modified to allow immersion of a cylindrical TE_{110} cavity into the cold gas flow. All spectra were taken with $\mathbf{B}_1 \perp \mathbf{B}$ as the $\mathbf{B}_1 \parallel \mathbf{B}$ configuration was not available. The DC magnetic field was calibrated with a NMR gaussmeter.

Mössbauer spectra were recorded using a constant acceleration spectrometer. Isomer shifts are quoted relative to iron metal at 300 K. The data were fitted with a sum of Lorentzians by using a least-squares routine.

Magnetization measurements were made using a SQUID S.H.E. VTS-50 magnetometer, with temperature uncertainties <0.1 K. Equivalent EPR and magnetic susceptibility samples were prepared in an argon atmosphere using D_2O as the solvent. The samples were stored in liquid nitrogen and transferred from liquid nitrogen into the helium bath of the magnetometer as quickly as possible (~1 min).

Computer simulations were written in FORTRAN and run on a CDC Cyber 175 computer. Depending on the simulation criteria, the program took 1–200 s of CPU time to run.

THEORY

Non-Kramers doublets

The quintet energy levels of the high-spin ferrous ion are usually parameterized in terms of the spin Hamiltonian (20):

$$\mathcal{H}_s = D(S_z^2 - 2) + E(S_x^2 - S_y^2) + \beta\,\mathbf{B}\cdot\mathbf{g}\cdot\mathbf{S}, \qquad (3)$$

where the first two terms represent the zero-field splitting. D and E parameterize the spin energy levels in zero field and reflect on the symmetry of the metal's environment. The exact eigenfunctions and energies of Eq. 3 in zero field are

$$\begin{aligned}
|2^{s'}\rangle &= a^+(|+2\rangle + |-2\rangle)/\sqrt{2} + a^-|0\rangle \\
|2^a\rangle &= (|+2\rangle - |-2\rangle)/\sqrt{2}, \\
|1^s\rangle &= (|+1\rangle + |-1\rangle)/\sqrt{2}, \\
|1^a\rangle &= (|+1\rangle - |-1\rangle)/\sqrt{2}, \\
|0'\rangle &= a^-(|+2\rangle + |-2\rangle)/\sqrt{2} - a^+|0\rangle,
\end{aligned}$$

$$\begin{aligned}
E_{2s'} &= 2(D^2 + 3E^2)^{1/2} \\
E_{2a} &= 2D \\
E_{1s} &= -D + 3E \\
E_{1a} &= -D - 3E \\
E_{0'} &= -2(D^2 + 3E^2)^{1/2},
\end{aligned} \qquad (4)$$

where $a^\pm = ((1 \pm D/(D^2 + 3E^2)^{1/2})/2)^{1/2}$. For the cases of interest D is large (typically $D \approx 10$ cm^{-1}), and for $E \ll D$ the quintet splits into two doublets, $|2^{s'}\rangle$, $|2^a\rangle$ and $|1^s\rangle$, $|1^a\rangle$, respectively, and a singlet, $|0'\rangle$. No interdoublet or doublet to singlet transitions are observed with standard EPR instrumentation ($h\nu \approx 0.3$ cm^{-1}, $B_{max} < 1.5$ T) as the Zeeman interaction is $\langle \mathcal{H}_{zee} \rangle < D$. Thus, the non-Kramers doublets are isolated and can be treated independently. In the limit of $E/D = 1/3$, on the other hand, the splitting between the states $|2^{s'}\rangle$ and $|2^a\rangle$, $\Delta_2 = 2D(2/\sqrt{3} - 1) = 0.3094D$, is the same as that between the states $|1^a\rangle$ and $|0'\rangle$, and if the condition $\Delta_2 < h\nu$ is satisfied, EPR signals may be observable with $\mathbf{B}_1 \perp \mathbf{B}$ for transitions between $|0'\rangle$ and $|1^a\rangle$ as well. Two previous reports (2, 20) have treated the rhombic term E of Eq. 3 with perturbation theory. This approach is inappropriate in ferrous complexes for two reasons. (*a*) Matrix elements involving E may easily exceed 10% of the value of those involving D, causing the perturbation results to be inaccurate. (*b*) A simple 2 × 2 diagonalization provides exact energy levels and spin wavefunctions for zero magnetic field. The case with magnetic field $B \neq 0$ is then straightforward.

A magnetic field **B** will increase the splitting of the non-Kramers doublets quadratically as shown in Fig. 1. The eigenfunctions for both doublets at resonance can be written as

$$|k^\pm\rangle = \alpha_k^\pm|k^{s(')}\rangle \pm \alpha_k^\mp|k^a\rangle, \qquad (5)$$

where $k = 1, 2$ label the $|1^\pm\rangle$ and $|2^\pm\rangle$ doublets, respectively, $\alpha_k^\pm = ((1 \pm \Delta_k/h\nu)/2)^{1/2}$, and Δ_k is the splitting of the doublet in zero field, $\Delta_1 = 6E$ and $\Delta_2 = 2[(D^2 + 3E^2)^{1/2} - D]$. The notation $|k^{s(')}\rangle$ refers to the states $|2^{s'}\rangle$ or $|1^s\rangle$ of Eq. 4. To observe resonance, the condition $\delta\epsilon = h\nu$ must be satisfied. From the energy splittings given in Fig. 1, the resonance condition is

$$(h\nu)^2 = \Delta_k^2 + (\tilde{g}_k\beta B_r)^2, \qquad (6)$$

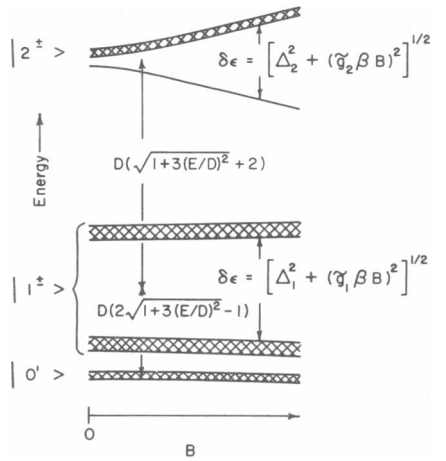

FIGURE 1 Energy levels of a quintet ($S = 2$) state for the case $D \gg E$, $g_{zz}\beta B$, and $D > 0$. The width of energy levels represents a spread in the value of E. The states $|1^{\pm}\rangle$ and $|2^{\pm}\rangle$ of the two non-Kramers doublets are eigenfunctions of Eq. 3 as defined in Eq. 5.

where $g_k = 2kg_{zz}a_k \cos\theta$, $a_1 = 1$, and $a_2 = a^+$. The angle between **B** and the z-axis of the molecular frame defined by Eq. 3 is θ, and B_r is the magnitude of the external magnetic field necessary for resonance. The azimuthal angle ϕ between the x-axis of Eq. 3 and **B** does not significantly affect the resonance condition as terms involving ϕ are second order perturbations. This fact can be seen upon inspection of the zero-field states of Eq. 4. In first order the x or y Zeeman components can only give finite matrix elements from states differing by $m_s = \pm 1$, but the states of the doublets have m_s-values which differ by 0, ± 2, ± 4.

A quantum of energy $h\nu$ can be exchanged with the microwave field $\mathbf{B}_1 \cos(2\pi\nu t)$ if the matrix elements $\langle k^{\pm}|\mathbf{B}_1 \cdot \mathbf{g} \cdot \mathbf{S}|k^{\mp}\rangle$ do not vanish. The matrix elements $\langle k^{\pm}|s_{\pm}|k^{\mp}\rangle$ are zero, thus the selection rules for EPR signals from Kramers centers, $\delta m_s = \pm 1$, will not give transitions. Interdoublet transitions obeying $\delta m_s = \pm 1$ have been observed in the far infrared (21–23). A nonzero transition probability occurs for $\mathbf{B}_1$ having finite projection on the z-axis as the matrix elements $\langle k^{\pm}|S_z|k^{\mp}\rangle$ are nonzero. A finite matrix element $\langle k^{\pm}|S_z|k^{\mp}\rangle$ strictly implies the selection rule $\delta m_s = 0$ and not $\delta m_s = \pm 2$, ± 4, ± 8 which have appeared in the literature (6, 24, 25). The use of $\delta m_s > 1$ implies multiple quantum transitions due to finite matrix elements of $\langle \pm|S_{\pm}^n|^{\mp}\rangle$ for $n \geq 2$. Using the golden rule (26) we find the transition probability induced by the microwave field at frequency ν_c to be

$$W_k(\nu) = (g_{zz}\beta B_{1z}/\hbar)^2 |\langle k^+|S_z|k^-\rangle|^2 f(\nu - \nu_c), \quad (7)$$

where $f(\nu - \nu_c)$ is a normalized lineshape function for a spin-packet.

A typical EPR experiment will sweep the magnetic field **B** using a fixed frequency ν_c. It is convenient, therefore, to use a lineshape function normalized with respect to field, $\int h(B)\mathrm{d}B = 1$, but use of Eq. 7 requires $\int f(\nu)\,\mathrm{d}\nu = 1$ (27). Thus we make a transformation to magnetic field variable B and the result is

$$W_k(B) = (g_{zz}\beta B_{1z}/\hbar)^2 |\langle k^+|S_z|k^-\rangle|^2 \cdot h(B - B_r)(\mathrm{d}B/\mathrm{d}\nu)|_{B=B_r}. \quad (8)$$

Evaluation of the matrix element gives

$$|\langle k^+|S_z|k^-\rangle|^2 = (ka_k\Delta_k(B_r, \theta)/h\nu_c)^2. \quad (9)$$

We have not found the conversion of frequency-swept to field-swept spectra in non-Kramers systems in the literature (2, 20).

The lineshape function $h(B)$ represents a spin-packet in magnetic field space. The width of $h(B)$ depends on the transverse spin relaxation time T_2 and on the resonance field. Few experimental measurements of the relaxation rates of ferrous complexes exist. NMR (28) and Mössbauer (29, 30) experiments find relaxation times for transitions between the quintet spin states in the range 10^{-7} to 10^{-4} s at $T \approx 4$ K.

To make an estimate of the width σ_B of $h(B)$ we use $\sigma_B = (\mathrm{d}B/\mathrm{d}\nu)\sigma_\nu$ and Eq. 6. For relaxation times $T_2 \approx T_1 = 1\ \mu$s, $\theta = 0°$, $\nu = 9$ GHz, and $B = 30$ mT, the width is $\sigma_B < 0.1$ mT. In comparison with other broadening mechanisms, the spin-packet linewidth is small, and for simplicity we therefore approximate the lineshape function with $h(B - B_r) = \delta(B - B_r)$. At low magnetic fields the δ-function approximation will not hold, however, as $h(B)$ will be broad and asymmetric near $B_r = 0$ due to the quadratic dependence of the resonance field on frequency. Combining Eqs. 8 and 9 and using Eq. 6 to calculate $\mathrm{d}B/\mathrm{d}\nu$, we have

$$W_k(B) = \frac{1}{4\hbar^2}\frac{B_{1z}^2\Delta_k^2(B_r, \theta)}{B_r\nu_c\cos^2\theta}\delta(B - B_r), \quad B_r \gg \sigma_B. \quad (10)$$

Notice that Eq. 10 diverges when the resonance field B_r approaches zero.

The lineshape model discussed so far follows from the spin Hamiltonian, Eq. 3, and time-dependent perturbation theory. It predicts the angular dependence of the resonance field correctly, as we have shown for single crystals of iron-doped zind fluosilicate (10), but it underestimates the line width. The dominant source of line broadening is thought to be a spread in the zero-field energy levels; it is indicated in Fig. 1 by a finite width of the levels. An analogous broadening, g-strain, is observed in Kramers systems (31) and a comparison to non-Kramers systems will be discussed for myoglobin.

The excess broadening in integer-spin EPR was first

noted by Bleaney and Scovil in their work on lanthanides in ethyl sulfates (32). Baker and Bleaney (33) tried to model the broadening by adding the ad hoc terms $\Delta_x S_x + \Delta_y S_y$ to a spin Hamiltonian without the quadratic terms DS_z^2 and $E(S_x^2 - S_y^2)$. Both Δ_x and Δ_y were assumed to be random variables. These extra terms give rise to an energy splitting of the correct form, Eq. 6, with $\Delta_k^2 = \Delta_x^2 + \Delta_y^2$, but they violate time reversal invariance and give rise to finite expectation values of S even in the absence of a magnetic field. Griffith (34) furthermore argued that one of the random variables could be eliminated by proper choice of basis, thus the model of Baker and Bleaney is unfounded.

The splitting in zero field, Δ_k, is not necessarily a proper random variable; a better choice might be to adopt a crystal field model of the ferrous ion with the electrostatic potentials that split the ^5D orbitals serving as random variables. In the analogous case of the high-spin ferric ion Levin and Brill used a distribution of the ^4P orbital energies to model the zero-field splitting of spin $S = 5/2$ metmyoglobin (35, 36). They showed that a Gaussian energy distribution of the ^4P levels leads to a skewed symmetric distribution in the zero-field parameters D and E of Eq. 3. Relating the zero-field splitting Δ_k to the electrostatic potential of the crystal field model requires at least three more parameters, and for simplicity we will stay in the framework of the spin Hamiltonian formalism. In the following we will assume Gaussian distributions of the zero-field parameters D and E keeping in mind that skew symmetric distributions might be more realistic. The origin of the zero-field parameter distributions, whether intrinsic and/or artifactual, is not clear. However, such distributions must be an ensemble property in contrast to lifetime broadening or superhyperfine interactions which are intrinsic to each molecule.

Simulation of integer-spin spectra

For fixed angle θ, a spread in the energy splitting Δ_k will result in a family of resonance curves described by Eq. 6 as shown in Fig. 2 *a*. Molecules with $\Delta_k^{(0)} > h\nu_c$ cannot satisfy the resonance conditions at any magnetic field, thus only a fraction of the molecules contribute to the EPR spectrum.

A single crystal spectrum is composed of many overlapping signals of lineshape $h(B - B_r)$ centered at $B_r^{(1)}$, $B_r^{(2)}$, $B_r^{(3)}$, etc. (refer to Fig. 2 *a*). Now suppose that the probability of a molecule having rhombicity in the interval E to $E + dE$ is $P(E)dE$ and the distribution of D values is sharp. The contribution of each spin-packed to the total spectrum at a field B to $B + dB$ is then $W_k(B)P(E)dB_r dE$. Using Eq. 10, an integration over B_r, and the transformation of variables E to B, we find the spectral intensity as a

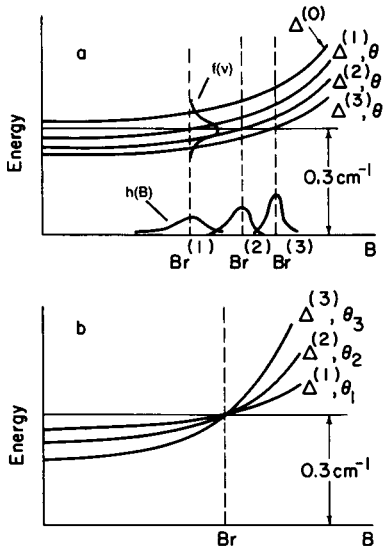

FIGURE 2 (*a*) Energy splitting $\delta\epsilon$ of a non-Kramers doublet as a function of magnetic field, B, for various values of the zero-field splitting $\Delta^{(i)}$ at a fixed angle θ. The symmetric Lorentzian spin packets, $f(\nu)$, in energy space broaden asymmetrically to give $h(B)$ in magnetic field space. No resonance will be observed from spin centers having $\Delta^{(0)} > 0.3$ cm^{-1} with an X band spectrometer. (*b*) Energy splitting $\delta\epsilon$ as a function of field, B, for a family of non-Kramers doublets having appropriate values of Δ and angle θ so as to resonant at magnetic field B_r.

function of magnetic field B to be

$$I_{k\theta}(B) = \frac{n(T, \nu_c)}{\nu_c} k(g_{zz}\beta/\hbar)^2 B_{1z}^2 |E| P(E), \qquad (11)$$

where $n(T, \nu_c)$ is the temperature-dependent population difference of the resonance states. Note that $n(T, \nu_c)$ is approximately linear in ν_c for a Boltzmann population of states, thus $I_{k\theta}(B)$ is almost independent of the microwave frequency. As mentioned above, we use a Gaussian distribution to represent the spread in zero-field parameters. Fig. 3 shows plots of $I_{k\theta}(B)$ for $\theta = 0°$ and $\theta = 60°$ with various widths σ_E and centers E_0 of $P(E) = (1/(2\pi)^{1/2}\sigma_E) \exp\{-[(E - E_0)/\sqrt{2}\sigma_E]^2\}$. If we consider an isolated non-Kramers doublet and assume g_{zz} to be known, then the only adjustable parameter in Eq. 11 is the rhombicity E. Therefore, we can in principle determine the exact nature of the zero-field distribution $P(E)$ from an experimental spectrum of a single crystal.

We also want to simulate powder spectra, because protein crystals are not always available and can have properties differing from the protein in solution. At a given magnetic field B, the powder spectrum is composed of signals from many different molecular orientations and zero-field parameters, as shown in Fig. 2 *b*. If we assume random molecular orientations, the contribution to the

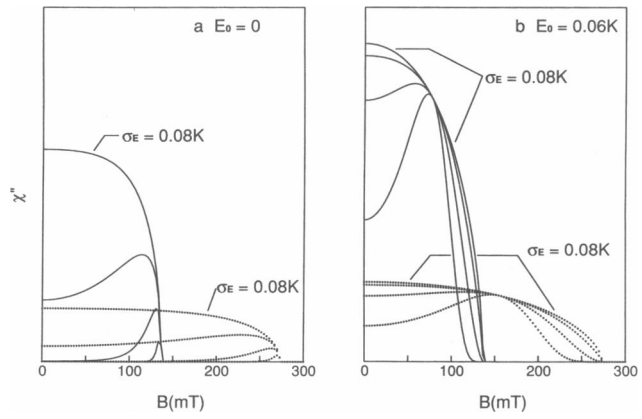

FIGURE 3 Spectral intensity, $\chi'' \sim I_{k\theta}(B)$, from Eq. 11 for center E-values (*a*) $E_0 = 0$ and (*b*) $E_0 = 0.06$ K. Each graph contains two sets with $\theta = 0°$ (_) and 60° (. . .), respectively, of four curves with distribution widths $\sigma_E = 0.01, 0.02, 0.04$, and 0.08 K (curves with largest $\chi''(B = 0)$ have $\sigma_E = 0.08$ K). We have assumed the orientation $\mathbf{B}_1 \parallel \mathbf{B}$, $k = 1$, $g_{zz} = 2.38$, and $\nu_c = 9.1$ GHz. The parameters are close to those used for simulation of the iron doped zinc fluosilicate spectra. 1 cm^{-1} = 1.439 K.

intensity at field B to $B + dB$ is $W_k(B)P(E)dB_r \cdot dE \sin\theta d\theta$, and from Eq. 11 the spectral intensity is

$$I_k(B) = \frac{n(T, \nu_c)}{\nu_c} k(g_{zz}\beta/\hbar)^2 \cdot \int_{\theta(B)} B_{1z}^2 |E| P(E) \sin\theta' \, d\theta'. \quad (12)$$

The integral is constrained by the resonance condition and a closed form expression has not been found. However, Eq. 12 can be evaluated numerically, for example with a contour method (37). Distributions in both D and E are handled analogously. Unless noted, the spectral simulations in this paper are generated with diagonalization of the 5 × 5 quintet representation of $\mathcal{H}_s$. The g values for each diagonalization point are determined to second order in spin-orbit coupling with Eq. 2 of reference 10.

Parallel vs. perpendicular B_1 orientation

EPR spectra of non-Kramers systems can be observed with either $\mathbf{B}_1 \parallel \mathbf{B}$ or $\mathbf{B}_1 \perp \mathbf{B}$. According to Eq. 7 the transition probability is proportional to B_{1z}^2, where B_{1z} is the component of $\mathbf{B}_1$ along the molecular z-axis. The signal intensities $W_k^\perp$ and $W_k^\parallel$ for $\mathbf{B}_1 \perp \mathbf{B}$ and $\mathbf{B}_1 \parallel \mathbf{B}$, respectively, are therefore related by

$$W_k^\perp(B) = W_k^\parallel(B) \overline{\sin^2(2\pi\nu_c t)} \tan^2\theta, \quad (13)$$

where the time averaged quantity $\sin^2(2\pi\nu_c t)$ equals ½.

In principle, $\mathbf{B}_1 \parallel \mathbf{B}$ is preferable for integer-spin systems. As indicated in Fig. 3 for a single crystal, $I_{k\theta}(B)$, is largest for $\theta = 0$; for randomly oriented molecules typical simulations show peak values of $d\chi''/dB$ that are roughly a factor of three larger for $\mathbf{B}_1 \parallel \mathbf{B}$ than for $\mathbf{B}_1 \perp \mathbf{B}$, where B_1 and all other parameters are kept the same. In practice, the latter condition may not apply. In the dual mode cavity described under Methods, for instance, B_1 and the filling factor depend on the $\mathbf{B}_1$ orientation.

The $\mathbf{B}_1 \parallel \mathbf{B}$ orientation not only enhances the signal-to-noise ratio of non-Kramers doublets, but it also attenuates impurity signals due to Kramers doublets. The transition probability vanishes for the latter in parallel field, $\mathbf{B}_1 \parallel \mathbf{B}$, as can be seen from Eq. 3.10b of reference 20. In practice, $\mathbf{B}_1$ is not perfectly parallel to $\mathbf{B}$ due to misalignment and finite sample size, and typical attenuation factors for the cavity described in the Methods section range from 200 to 1,000. Ideally, spectra should be observed with both $\mathbf{B}_1$ orientations to verify that Eq. 13 applies, as agreement with Eq. 13 is clear proof of an integer-spin system.

Quantitation

We have obtained quantitative agreement of spin counts between various samples using two methods. As usual, we compare the spectrum of a standard sample having a known number of spins, N_{std}, with that of a sample having an unknown number of spins, N_x. Since non-Kramers EPR signals at X band usually represent only a fraction of the spins, the quantitation has to rely on simulations. Method 1 relates the amplitudes of the simulated spectra, S_{std} and S_x, to the corresponding features E_{std} and E_x (usually zero-to-valley) of the experimental spectra, where E is adjusted for gain, microwave power, population difference, etc. The unknown number of spins of a sample then is

$$N_x = N_{std}(E_x/E_{std})(S_{std}/S_x). \quad (14)$$

Concentration may be used in place of spin count N.

Method 2 uses double integration of $d\chi''/dB$ to determine the unknown number of spins relative to a standard, where the standard may be a Kramers center. The net microwave power absorbed at resonance, due to transitions between states $|i\rangle$ and $|j\rangle$, is

$$dP_{ij} = (2\pi\nu\beta^2/\hbar)n(T, \nu_c) \cdot |\langle i|\mathbf{B}_1 \cdot \mathbf{g} \cdot \mathbf{S}|j\rangle|^2 f(\nu - \nu_c) dN(\theta, \phi\, D, E), \quad (15)$$

where $dN(\theta, \phi\, D, E)$ is the number of spins obeying the resonance condition, Eq. 6. We shall now derive expressions for the total number of spins of Kramers and non-Kramers centers.

For Kramers centers, we assume the lineshape function

and zero-field parameter distributions are sharp. The spectrum for a field-swept experiment of an axially symmetric site is then

$$I^{KR}(B)dB = (\pi\alpha N_0\nu_c/\hbar)n(T,\nu_c)\beta^2 \cdot |\langle i|\mathbf{B}_1 \cdot \mathbf{g} \cdot \mathbf{S}|j\rangle|^2\delta(B - B_r)(dB/d\nu)d\cos\theta, \quad (16)$$

where α is an instrumental constant and N_0 is the total number of spins. For simplicity, we shall replace the transition probability with an angle independent average (27). Thus, for an effective spin $S' = \frac{1}{2}$ signal,

$$\beta^2|\langle i|\mathbf{B}_1 \cdot \mathbf{g} \cdot \mathbf{S}|j\rangle|^2 dB/d\nu = \beta h B_1^2 g_{ave}/4, \quad (17)$$

where g_{ave} is given by Eq. 6 of reference 27 and h is Planck's constant. Combining Eqs. 16 and 17, and integrating gives the total number of spins for a Kramers center,

$$N_0^{KR} = \frac{1}{\alpha\pi^2\nu_c\beta B_1^2 n(T,\nu_c)g_{ave}} \int I^{KR}(B)\,dB. \quad (18)$$

For a non-Kramers center the problem is immediately complicated by the effects of the zero-field parameter distribution. For simplicity, we assume the distribution in D-values is sharp (a distribution of D-values will not affect the lineshape of the $k = 1$ non-Kramers doublet, because the splitting in zero field, $\Delta_1 = 6E$, does not depend on D) and concentrate on determining N_0 for a single crystal. From Eq. 15, the field-swept spectrum for a non-Kramers center is

$$I_{k\theta}^{NK}(B)dB = (2\pi\alpha N_0\nu_c/\hbar)n(T,\nu_c)\beta^2 \cdot |\langle i|\mathbf{B}_1 \cdot \mathbf{g} \cdot \mathbf{S}|j\rangle|^2\delta(B - B_r)(dB/d\nu)P(E)dE. \quad (19)$$

Combining Eqs. 9 and 19, and integrating gives the number of spins for a non-Kramers center,

$$N_0^{NK} = \frac{h}{\alpha\pi^2 B_1^2 n(T,\nu_c)} \int I_{k\theta}^{NK}(B)(B/\Delta_k^2)\,dB, \quad (20)$$

where we have assumed $\mathbf{B}_1 \parallel \mathbf{B}$. The splitting in zero field, Δ_k, can be calculated for each spectral point with Eq. 6. Eqs. 18 and 20 allow quantitation of an unknown sample concentration relative to a standard that may be either a Kramers or non-Kramers center.

RESULTS

Iron-doped zinc fluosilicate

X band EPR spectra and simulations of a single crystal of (Zn/Fe)FS are displayed in a previous paper [10].[1] A broad negative dip from the $|1^{\pm}\rangle$ doublet of a quintet is observed with a turning point at $B \approx 140$ mT. Simulations suggest that 60% of the molecules satisfy the inequality $\Delta_1 < h\nu$. To test integration method 2, we compared the spin counts of a (Zn/Fe)FS crystal against a frozen solution of metMb. The number of iron atoms in the crystal was determined from the crystal dimensions and the unit cell volume (38); the concentration of iron in the solution of metMb was determined optically using $\epsilon_{410} = 157\ cm^{-1}\ mM^{-1}$. The spectra were integrated to give χ'', then integrated a second time in accordance with Eq. 18 for metMb or Eq. 20 for (Zn/Fe)FS. Taking the metMb sample as the standard, the predicted number of iron atoms in the (Zn/Fe)FS sample was found to be within 15% of the known number.

Q band EPR spectra and simulations of a single crystal of (Zn/Fe)FS are shown in Fig. 4. All molecules have $\Delta_1 < h\nu$ as at $B = 0$ we find $\chi'' = 0$. The lineshapes are poorly defined because of the low sensitivity of the spectrometer. The eight-line cobalt impurity signal,

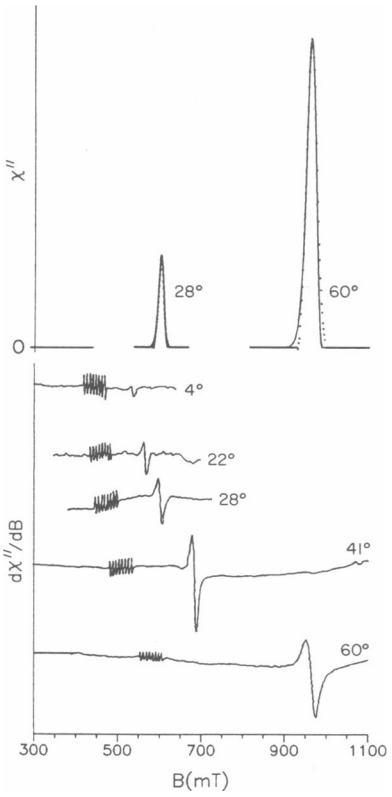

FIGURE 4 Q band (35 GHz) EPR spectra and simulations of a single crystal of 4% (Fe/Zn)FS at $T = 15$ K and various angles θ using $\mathbf{B}_1 \perp \mathbf{B}$. The absorption spectra χ'' (. . .) are numerical integrations of the appropriate $d\chi''/dB$ spectra. Simulation parameters: $E_0 = 0.06$ K, $\sigma_E = 0.014$ K, $g_{zz} = 2.38$. Instrumental parameters: microwave, 35.00 GHz at 7 mW; modulation, 100 kHz at 2 mT_{pp}; gain, 200; dB/dt, 8.3 mT/s; filter, 0.1 s. The octet signal at $B \approx 500$ mT is from a cobalt impurity.

[1]The number of spins stated in Fig. 2 of reference 10 should be 7×10^{17}, not 10^{16}.

which was seen at X band as well (10), is relatively strong since the spectrometer operated with $\mathbf{B}_1 \perp \mathbf{B}$. In the upper part of Fig. 4, simulations of χ'' for two orientations are overlaid on the integrated data. The simulation parameters are given in the figure caption; the best value of the Gaussian width, $\sigma_E = 0.014$ K, is considerably smaller than that required to simulate the X band data, $\sigma_E = 0.06$ K. In view of the low quality of the Q band spectra it is not clear yet if these differences in σ_E are significant.

Hexaquo Fe^{+2}

Fig. 5 shows EPR spectra of a frozen solution of 10 mM iron sulfate prepared under argon and quenched in liquid nitrogen. The lineshape did not change noticeably when the concentration was reduced by a factor of 4, thus we conclude the samples were magnetically dilute (i.e., magnetic dipole interactions between iron atoms were negligible). In addition, no significant lineshape difference was observed from a sample with 50% glycerol. A significant lineshape change in the low field region ($B < 80$ mT) of the spectra is observed, however, when the microwave power is raised to 200 mW at 4 K or 2 mW at 2 K, suggesting partial saturation of the signal.

The troughs of $d\chi''/dB$ of Fig. 5 correspond to an effective g-value of 8 suggesting that the signals are due to resonance from the $|2^{\pm}\rangle$ doublet. The assignment is supported by the simulations shown in Fig. 5,[2] and we find quantitative agreement of the relative signal intensities between the $\mathbf{B}_1 \parallel \mathbf{B}$ and $\mathbf{B}_1 \perp \mathbf{B}$ orientations, i.e., Eq. 13 is obeyed after correction for differences in microwave power and the filling factor. Attempts to simulate the spectra under the assumption of resonance from the $|1^{\pm}\rangle$ doublet, however, were unsuccessful. For temperatures $T < 20$ K the EPR signal intensity is inversely proportional to temperature; thus the resonance is from a ground state spin doublet. An accurate D value measurement from depopulation studies of the doublet can not be made as the lineshape changes near 30 K. A reassessment of the baseline position in our earlier work (10) has changed the parameter set of best fit to $D = -8$ K, $E_0 = -2.05$ K, $\sigma_E = 0.6$ K.

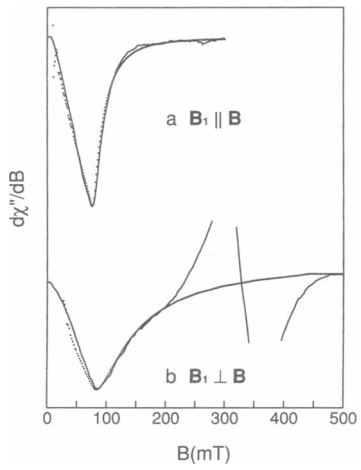

FIGURE 5 EPR spectra (_) and simulations (. . .) of a frozen aqueous solution of 10 mM $FeSO_4$ at $T = 4$ K using (a) $\mathbf{B}_1 \parallel \mathbf{B}$ and (b) $\mathbf{B}_1 \perp \mathbf{B}$. Simulation parameters: $D = -8$ K, $E_0 = -2.05$ K, $\sigma_E = 0.60$ K, $\mathbf{g}_e$ = (2.00, 2.06, 2.14). $\mathbf{g}_e$ represents the g tensor values calculated with second order spin-orbit coupling using zero-field parameters D and E_0 (10). Instrumental parameters: microwave, 9.1 GHz at 2 mW (unsaturated); modulation, 100 kHz at 0.8 mT_{pp}; gain, 4×10^5; dB/dt, 3.3 mT/s; filter, 0.5 s. The large signal in the field range $200 < B < 500$ mT for $\mathbf{B}_1 \perp \mathbf{B}$ is from a ferric impurity.

TABLE 1 Quadrupole splitting ΔE_q, isomer shift δ_{Fe}, and line width Γ in millimeters per second of a frozen solution of 10 mM $FeSO_4$

T	ΔE_q	δ_{Fe}	Γ
K			
4.2	3.36	1.40	0.42
100	3.34	1.38	0.42
150	3.28	1.34	0.40
200	3.21	1.32	0.45

Upon temperature cycling of a frozen solution of $FeSO_4$ from 4 to 200 K and back to 4 K, the $S = 2$ EPR signal changed in shape and intensity. A magnetic susceptibility measurement of a sample treated exactly in the same manner showed no change.

The results of Mössbauer measurements on a frozen aqueous solution of 10 mM $FeSO_4$ in zero field as a function of temperature are given in Table 1.

The spin quantitation of a $FeSO_4$ solution sample with known Fe^{+2} ion concentration was compared with the Fe^{+2} ion count of the (Zn/Fe)FS crystal via quantitation methods 1 or 2. The predicted concentration found for $FeSO_4$ was only 35% of the actual value, thus the agreement is not good. Most of the error presumably comes from the uncertainty in the fraction of ions that satisfy the condition $\Delta_2 < h\nu$ and thus are observable by EPR. For the parameter set adopted in Fig. 5 this fraction is ~5% only.

EPR measurements on frozen solutions of 10 mM $FeCl_2$ were also performed. Surprisingly, a significant difference between $FeSO_4$ and $FeCl_2$ is observed in both

[2]The noise in the simulations at low magnetic field is a consequence of the inverse B dependence of the transition probability, Eq. 10. Simulations with less noise near $B = 0$ can be generated using perturbation theory, but the inaccuracies of the perturbation method have yet to be determined.

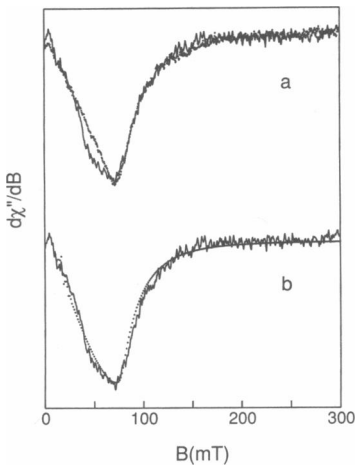

FIGURE 6 (*a*) EPR spectra of frozen aqueous solutions of 10 mM $FeCl_2$ (_) and 10 mM $FeSO_4$ (. . .) at $T = 4$ K using $\mathbf{B}_1 \parallel \mathbf{B}$. The amplitude of the $FeSO_4$ signal is artificially reduced by 20% to demonstrate lineshape differences. (*b*) Overlay of the $FeCl_2$ spectra in (*a*) with simulation (. . .). Simulation parameters: $D = -8$ K, $E_0 = -2.05$ K, $\sigma_E = 0.52$ K, $\mathbf{g}_e = (2.00, 2.06, 2.14)$. Instrumental parameters: microwave, 9.12 GHz at 2 mW (unsaturated); modulation, 100 kHz at 0.8 mT_{pp}; gain, 10^6; dB/dt, 2 mT/s; filter, 0.5 s.

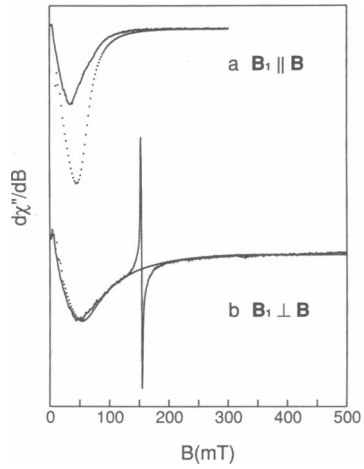

FIGURE 7 EPR spectra (_) and simulations (. . .) of a frozen aqueous solution of 10 mM FeEDTA in 75% glycerol at $T = 4$ K using (*a*) $\mathbf{B}_1 \parallel \mathbf{B}$ and (*b*) $\mathbf{B}_1 \perp \mathbf{B}$. Simulation parameters: $D = -13$ K, $E_0 = -1.50$ K, $\sigma_E = 0.15$ K, $\mathbf{g}_e = (2.00, 2,04, 2.20)$. Instumental parameters: microwave, 9.109 GHz (*a*) or 9.142 (*b*) at 2 mW (unsaturated); modulation, 100 kHz at 0.8 mT_{pp}; gain, 5×10^5; dB/dt, 1.5 mT/s (*a*) or 2.5 mT/s (*b*); filter, 0.5 s (*a*) or 0.2 s (*b*). The ratio of signal strengths $\parallel/\perp$ of the simulations obeys Eq. 13 but does not match the data. The signal at $B = 150$ mT ($g = 4.2$) in $\mathbf{B}_1 \perp \mathbf{B}$ is a ferric impurity.

intensity and lineshape. The experiments were repeated many times on several different samples. A comparison is shown in Fig. 6 *a* of samples having concentrations of Fe^{+2} ion equal to within 3%, as determined by plasma emission and correction for Fe^{+3} impurity by EPR quantitation. The $FeCl_2$ spectrum of Fig. 6 *b* is 20% weaker and slightly broader. Good simulations of the $FeCl_2$ spectra are found with the parameters $D = -8$ K, $E_0 = -2.05$ K, and $\sigma_E = 0.52$ K. The reduced intensity of the $FeCl_2$ spectrum is predicted by the simulation, but another parameter set with an equally good fit to the data was found that predicted the intensity of the $FeSO_4$ and $FeCl_2$ signals to be approximately equal. A sample of $FeCl_2$ with 75% glycerol did show a different EPR spectrum, resembling that of $FeSO_4$.

Iron(II) ethylenediaminetetraacetate (FeEDTA)

Experiments similar to those done on hexaquo Fe^{+2} were performed on ~10 mM aqueous solutions of FeEDTA. EPR and magnetic susceptibility results are shown in Figs. 7–9. No significant EPR lineshape difference was observed when the iron concentration was lowered by a factor of 4, thus the samples are magnetically dilute. In addition, no significant lineshape difference was observed from a sample with 75% glycerol. A least-square fit of the magnetic susceptibility data gives approximately the same zero-field splitting parameters, $D = \pm 13$ K and $E/D = 1/3$, as obtained for the frozen solution of $FeSO_4$ (10). (The sign of D is ambiguous at $E/D = 1/3$, where the zero-field term of the spin Hamiltonian can be written as

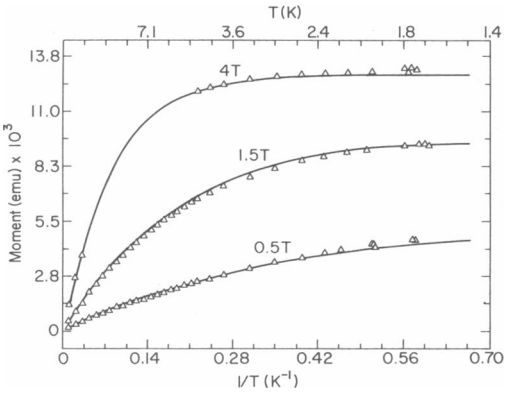

FIGURE 8 Magnetic susceptibility measurements and simulation of a frozen solution of 12 mM FeEDTA in D_2O at various magnetic fields. A least-square fit of the data to the spin Hamiltonian, Eq. 3, gave $D = \pm 13 \pm 1$ K, $E = \pm 4.3 \pm 0.5$ K, 0.92 ± 0.2 μmol of iron, $\mathbf{g} = (2.12\ 2{,}24, 2.00)$. The total iron content, determined by weight of sample ingredients, was 0.94 μmol.

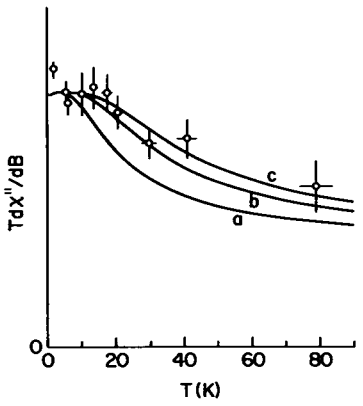

FIGURE 9 Temperature dependence of the FeEDTA EPR signal of Fig. 7 *a*. Signal intensity is determined from the depth of the valley at $B \approx 40$ mT. The temperature was determined from the known temperature dependence of an added metMb sample. The solid lines assume a Boltzmann population of levels with (*a*) $D = -10$ K, $E = -1$ K, (*b*) $D = -16$ K, $E = -1.2$ K, or (*c*) $D = -20$ K, $E = -1.4$ K.

$[2D/3][S_z^2 - S_y^2]$. A coordinate system rotation of 90° about the x axis will change the sign of D, but the two coordinate systems are indistinguishable in an unoriented sample.) In contrast, the EPR spectra of FeEDTA differ markedly from those of the $FeSO_4$ solution. The FeEDTA spectra are broader, have shifted to a lower magnetic field, and are approximately four times stronger.

The low field region ($B < 40$ mT) of the FeEDTA spectrum saturates with a microwave power of 0.2 mW at 4 K. At a temperature of 50 K, the EPR lineshape is unchanged relative to the unsaturated 4 K spectrum of Fig. 7, and signals are observable up to liquid nitrogen temperatures. FeEDTA is thus an exception, as all other compounds that we have studied give EPR signals which broaden or vanish at such high temperatures. A depopulation experiment of the FeEDTA signal was performed using metMb as a thermometer. The signal intensity as a function of temperature and fits assuming a Boltzmann distribution with the signal from the $|2^{\pm}\rangle$ ground doublet are shown in Fig. 9. The fits of the data in Fig. 9 suggest a larger value, $D = -16$ to -20 K, than that deduced from the susceptibility, but they show that the EPR signals are from a ground doublet.

Assuming the EPR signals are from the $|2^{\pm}\rangle$ doublet, the best simulation of spectra using $\mathbf{B}_1 \perp \mathbf{B}$ is obtained with $D_0 = -13$ K, $E_0 = -1.5$ K, and $\sigma_E = 0.15$ K. This parameter set corresponds to ~20% of the spins obeying the inequality $\Delta_2 < h\nu$ with X band EPR and thus predicts the increased signal intensity relative to the spectra of the hexaquo Fe^{+2}, where only ~5% have $\Delta_2 < h\nu$. Spectral simulations generated with the assumption of resonance from the $|1^{\pm}\rangle$ doublet were unsuccessful. As is evident from a comparison of Figs. 7, *a* and *b*, the same parameters fit the $\mathbf{B}_1 \parallel \mathbf{B}$ spectrum rather poorly; not only is the simulated intensity too large, but the trough of the simulation occurs at too high a field. The reason for this behavior is not yet understood, in fact all other spectra which were simulated well with one $\mathbf{B}_1$ orientation, could be simulated equally well with the other orientation, in obeyance of Eq. 13. Consequently, an EPR quantitation of samples having known concentrations gave poor agreement.

Mössbauer spectra of a frozen aqueous solution of 10 mM FeEDTA show two broad, asymmetrical lines indicative of sample inhomogeneity. A sample with 75% glycerol, however, gave sharp lines showing two components. Component one accounts for 72% of the total iron in the sample and component two accounts for 28%. The results of zero field measurements as a function of temperature are given in Table 2.

Model hemes

Fig. 10 shows polycrystal EPR spectra of the $S = 2$ model heme complex Fe(II) 2-methylimidazole meso-tetraphenylporphyrin (FeTPP) (15) in both cavity modes. The parallel field spectrum lacks the impurity signal of our previous work (10). Except for the ferric impurity signal of $g \approx 6$, the spectra are virtually identical to the $FeSO_4$ spectra and therefore the FeTPP resonance must be from the $|2^{\pm}\rangle$ doublet of the quintet. The spectra also vary with microwave power in the same way as that observed for the hexaquo Fe^{+2}. The relative signal intensity between the $\mathbf{B}_1 \parallel \mathbf{B}$ and $\mathbf{B}_1 \perp \mathbf{B}$ orientations are found to obey Eq. 13 within experimental error, after correction for differences in microwave power and filling factor.

The Fe-CO bond in the low-spin $S = 0$ model heme compounds Fe(II) imidazole protoporphyrin IX CO and Fe(II) 2-methylimidazole protoporphyrin IX CO can be photolytically cleaved (39), resulting in a high-spin $S = 2$ state. No EPR signals were observed during continuous illumination, however, presumably because of very rapid recombination of CO with the iron. We mention this negative result as a control experiment for the protein results to follow.

TABLE 2 **Mössbauer parameters of 10 mM FeEDTA in 75% glycerol**

T	$\Delta E_q^{(1)}$	$\delta_{Fe}^{(1)}$	$\Gamma^{(1)}$	$\Delta E_q^{(2)}$	$\delta_{Fe}^{(2)}$	$\Gamma^{(2)}$
K						
4.2	3.45	1.28	0.29	3.01	1.21	0.43
30	3.48	1.28	0.28	3.08	1.22	0.40
93	3.45	1.27	0.25	3.03	1.22	0.50
153	3.37	1.24	0.27	2.86	1.20	0.54
193	3.31	1.21	0.25	2.78	1.15	0.63

See Table 1 for explanation of symbols and units.

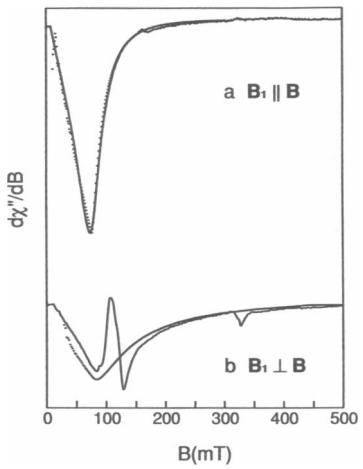

FIGURE 10 Polycrystal EPR spectra (_) and simulations (. . .) of Fe(II) 2-methylimidazole meso-tetraphenylporphyrin at T = 4 K using (a) $\mathbf{B}_1 \| \mathbf{B}$ and (b) $\mathbf{B}_1 \perp \mathbf{B}$. The signals at 140 mT and 330 mT in $\mathbf{B}_1 \perp \mathbf{B}$ are from half-integer-spin impurities. Simulation parameters: $D = -8$ K, $E = -2.05$ K, $\sigma_E = 0.60$ K, $g_e = (2.00, 2.06, 2.14)$. Instrumental parameters: microwave, 9.108 GHz (a) or 9.060 GHz (b) at 0.2 mW (unsaturated); modulation, 100 kHz at 0.8 mT_{pp}; gain, 1.25×10^5; dB/dt, 2.5 mT/s (a) or 3.5 mT/s (b); filter, 0.5 s. The intensity of the $\mathbf{B}_1 \perp \mathbf{B}$ spectrum is 10% smaller than expected from consideration of Eq. 13, but the uncertainty of the filling factor for a small dispersed, powder sample is large.

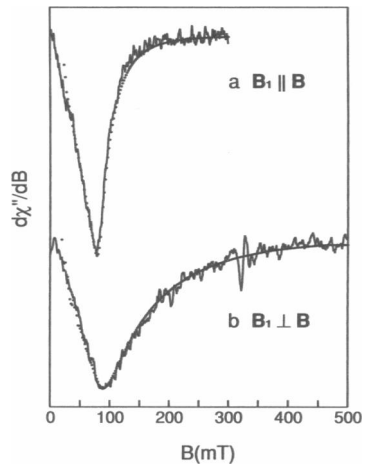

FIGURE 11 Difference (light-dark) spectra (_) and simulations (. . .) of a frozen solution of photodissociated carbonmonoxymyoglobin, Mb*(CO), at T = 4 K using (a) $\mathbf{B}_1 \| \mathbf{B}$ and (b) $\mathbf{B}_1 \perp \mathbf{B}$. Sample conditions: 10 mM Mb, 50% glycerol, 50 mM KP_i, pH = 7. Simulation parameters: $D_0 = 7$ K, $\sigma_D = 1.5$ K, $E_0 = 1.3$ K, $\sigma_E = 0.35$ K, $g_e = (2.07, 2{,}09, 2.00)$. Instrumental parameters: microwave, 9.093 GHz (a) or 9.140 GHz (b) at 2 mW (unsaturated); modulation, 100 kHz at 0.8 mT_{pp}; gain, 1.6×10^6; dB/dt, 1.5 mT/s (a) or 2.5 mT/s (b); filter, 1 s, 5 scans in 17 min. There is a subtraction artifact at $B = 330$ mT in $\mathbf{B}_1 \perp \mathbf{B}$.

Myoglobin (Mb)

In a previous paper we reported the first EPR spectra observed from quintet states of myoglobin (10). Fig. 11 shows difference spectra between the diamagnetic CO-adduct of Mb and its photolysis product Mb*(CO) with $\mathbf{B}_1 \| \mathbf{B}$ and $\mathbf{B}_1 \perp \mathbf{B}$. The lineshapes are not significantly affected by microwave powers of up to 2 mW at 2 K. In contrast, the lineshape of the photodissociated complex of Mb*(O_2) (10), which differs from that of Mb*(CO), is significantly altered with microwave power of 0.2 mW at 2 K. Good simulations of the spectra are obtained with the parameter set $D_0 = 7$ K, $\sigma_D = 1.5$ K, $E_0 = 1.3$ K, $\sigma_E = 0.35$ K and are overlaid on the data of Fig. 11. The relative signal intensity of the $\mathbf{B}_1 \| \mathbf{B}$ and $\mathbf{B}_1 \perp \mathbf{B}$ orientations are found to obey Eq. 13. The parameter set, which now invokes a spread in parameters D and E, is compatible with magnetic susceptibility (40) and far-infrared (22) results. However, the Mb spectra are similar to those of the hexaquo Fe^{+2} and FeTPP with the trough in $d\chi''/dB$ for Mb occurring 5 mT higher and being approximately a factor of three weaker than in the $FeSO_4$ spectra of Fig. 5. Thus, reasonably good simulations for Mb can be obtained also with $\sigma_D = 0$ and other parameters close to the set used for FeTPP or the hexaquo Fe^{+2}.

The high protein concentration and the formation of snowlike ice crystals upon freezing result in a relatively opaque sample. The addition of glycerol to the sample results in glass formation, allowing for deeper light penetration and presumably a larger fraction of photodissociated centers. Equivalent samples of MbCO with and without 50% glycerol showed no lineshape differences, but the signal intensity from the 50% glycerol sample was 2.5 times greater under identical illumination and other conditions. Thus the intensity of the Mb*(CO) signal with 50% glycerol is approximately equal to that of the frozen solution of $FeSO_4$, assuming that all MbCO molecules remain photodissociated during the measurements. Myoglobin in 75% glycerol undergoes what appears to be a glass phase transition at 180 K (41). However, EPR spectra of Mb*(CO) with 50% glycerol at 4 K, showed no difference before and after "annealing" at 200 K for 15 min.

Control EPR experiments were performed on the phosphate buffer used in the Mb samples. The EPR samples were prepared in the same manner as the deoxyMb and MbCO samples, except with no Mb. No significant EPR signals were found before or after illumination of the sample. Also, a frozen solution of aqueous $FeSO_4$ saturated with CO showed no EPR spectral differences before or after illumination.

We have checked for an EPR signal from the photolyzed complex of MbNO, which one might expect to give signals similar to Mb*(CO) or Mb*(O_2). The MbNO

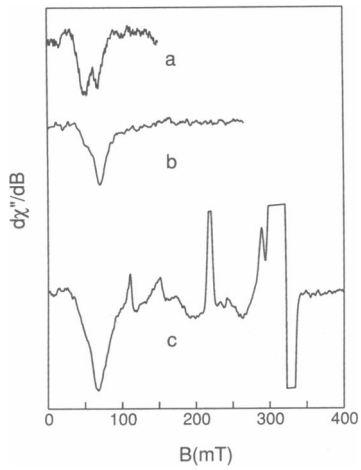

FIGURE 12 Frozen solution EPR spectra of cytochrome oxidase from (*a*) 0.35 mM yeast, $\mathbf{B}_1 \parallel \mathbf{B}$, (*b*) 0.23 mM bovine heart, $\mathbf{B}_1 \parallel \mathbf{B}$, and (*c*) bovine heart, $\mathbf{B}_1 \perp \mathbf{B}$, at $T = 4$ K. Instrumental parameters: microwave, 9.05 GHz (*a*, *b*) or 9.10 GHz (*c*) at 2 mW; modulation, 100 kHz at 1.1 mT_{pp} (*a*) or 0.8 mT_{pp} (*b*, *c*); gain, 3.75×10^6 (*a*) or 1.25×10^6 (*b*, *c*); dB/dt, 0.6 mT/s (*a*), 3.5 mT/s (*b*), or 2.5 mT/s (*c*); filter, 1 s.

complex has spin $S = \frac{1}{2}$ and gives an EPR signal which decreases in intensity proportionately to the number of Mb*(NO) centers created (42). Thus, by monitoring the intensity of the $S = \frac{1}{2}$ EPR signal with $\mathbf{B}_1 \perp \mathbf{B}$ during photolysis, it was clear that a sufficient concentration—comparable with the concentration of centers created in Mb*(CO) and Mb*(O_2) samples—of Mb*(NO) centers was created. Surprisingly, no integer-spin signal was observed.[3]

Cytochrome c oxidase

Integer-spin EPR signals have been reported from the Fe_{a3} Cu_B site of cytochrome *c* oxidase (C*c*O) of bovine heart (2, 7, 8). The signal, usually referred to as the "$g = 12$" resonance, has been reported with $\mathbf{B}_1 \parallel \mathbf{B}$ (2), but not simultaneously with $\mathbf{B}_1 \perp \mathbf{B}$ under identical conditions. Fig. 12 shows integer-spin spectra of the $Fe_{a3}Cu_B$ site using both field orientation, $\mathbf{B}_1 \parallel \mathbf{B}$ and $\mathbf{B}_1 \perp \mathbf{B}$. Note that the ratio of parallel to perpendicular signal intensity is significantly smaller in comparison to the other integer-spin complexes. In addition, Fig. 12 *a* shows a similar integer-spin signal from C*c*O of yeast. The spectrum from yeast appears to contain two components with minima at $B = 45$ mT and $B = 65$ mT. The lower field component is also weakly visible in the bovine heart sample. The magnitude (zero-to-trough) of the yeast signal is 20% of the bovine heart signal after scaling for gain and concentration.

[3]A number of other heme proteins were also checked for non-Kramers EPR signals at *X* band. No EPR signals were observed from the following complexes: single crystals of deoxyMb, photodissociated bovine hemoglobin CO, reduced and compound II complexes of horse radish peroxidase (HRP), photodissociated HRP CO, and reduced catalase. The lack of signals in some cases is presumably explained by the magnitudes of zero-field parameters which shift the EPR resonance out of the energy regime of an *X* band spectrometer, $\Delta_k > h\nu \approx 0.3$ cm^{-1}.

Azide complex of hemerythrin

EPR signals have been reported from the binuclear ferrous site of the azide complex of hemerythrin (3, 24). Fig. 13 shows EPR spectra using both field orientations, $\mathbf{B}_1 \parallel \mathbf{B}$ and $\mathbf{B}_1 \perp \mathbf{B}$. At low temperatures, the signal intensity is inversely proportional to temperature, indicating a ground state doublet as has been stated previously (24). The spectra clearly show lineshape changes when the microwave power is increased as shown in Fig. 14. The "saturation" at low field is a spectral characteristic of many, if not all ferrous complexes. The spectra of Fig. 14 and similar spectral changes at 4 K contradict a previous statement of no saturation at 200 mW and 4.2 K (24).

Extensive attempts at simulation of the spectra assuming a $S = 2$ spin Hamiltonian have been unsuccessful. It is possible to match the field value at the trough of $d\chi''/dB$ as by appropriate adjustment of D and E parameters the resonance can be positioned at any field $B < h\nu/\tilde{g}_k\beta$, where $\tilde{g}_k = 2kg_{zz}a_k$, but the shape of the simulation strongly depends on σ_E as well.

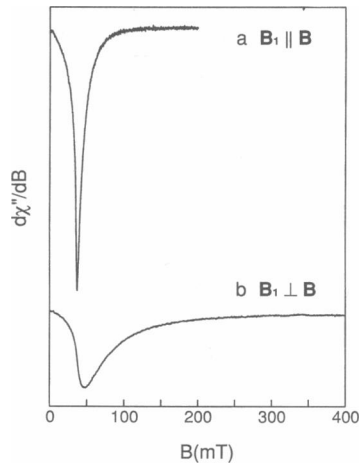

FIGURE 13 Frozen solution EPR spectra of the azide complex of deoxyhemerythrin from *Phascolopsis gouldii* at $T = 4$ K using (*a*) $\mathbf{B}_1 \parallel \mathbf{B}$ and (*b*) $\mathbf{B}_1 \perp \mathbf{B}$. Fe_2N_3 concentration is ~5 mM. Instrumental parameters: microwave, 9.059 GHz (*a*) or 8.993 GHz (*b*) at 2 μW (unsaturated); modulation, 100 kHz at 0.8 mT_{pp}; gain, 1.25×10^5; dB/dt, 2 mT/s; filter, 0.1 s (*a*) or 0.2 s (*b*).

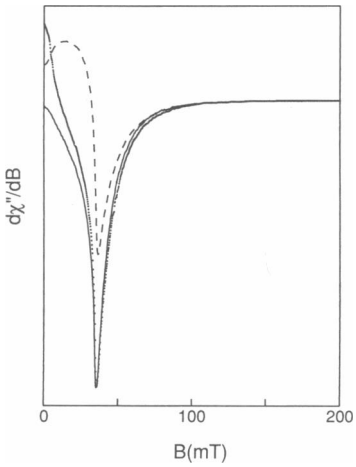

FIGURE 14 Power dependence of the EPR signal of the azide complex of deoxyhemerythrin at T = 2 K using $\mathbf{B}_1 \parallel \mathbf{B}$. Instrumental parameters: microwave, 9.059 GHz at 0.002 (_), 0.2 (. . .), or 20 mW (--); modulation, 100 kHz at 0.8 mT_{pp}; gain, 1.6×10^5 (_); dB/dt, 4 mT/s; filter, 0.5 s. Other gains adjusted relative to (_) in proportion with (microwave power)$^{1/2}$.

DISCUSSION

Iron doped zinc fluosilicate

As we have shown earlier (10), Eq. 11 reproduces the angular dependence of single-crystal EPR spectra of (Zn/Fe)FS and, with an appropriate choice of $P(E)$, it reproduces the spectral shape reasonably well. Here, moreover, we have demonstrated that the parameters of the simulation can be used to deduce the number of spins in a sample based on comparison with a known standard and on Eqs. 18 and 20. Specifically, we compared the numerical integrals of spectra of a metmyoglobin standard with that of a (Zn/Fe)FS single crystal and found a number of spins within 15% of the independently measured value. The earlier statement of Hagen (2) that integer-spin EPR spectra do not lend themselves to spin quantitation using numerical integration is therefore invalid. The quantitation clearly depends on the accuracy of the simulation, in particular on the assumed distribution of Δ_k-values, which determines the fraction of molecules observable at a given frequency through the inequality $h\nu > \Delta_k$. (Zn/Fe)FS is a particularly favorable case since EPR arises from the $|1^{\pm}\rangle$ doublet, thus the distribution of $\Delta_1 = 6E$ is given entirely by $P(E)$. In addition, the fraction of molecules observable at X band is 60%, a value that is large compared to all other cases considered here. Ideally, integer-spin EPR spectra should be taken at sufficiently high frequency so that the entire population of $S = 2$ molecules is observable. Experiments on (Zn/Fe)FS at 35 GHz satisfy this condition, but the quality of the preliminary spectra in Fig. 4 was inadequate for accurate quantitation. The simulations appear to require a smaller spread, σ_E, in $P(E)$ than deduced from X band data, and if better measurements confirm this observation, they could either imply a non-Gaussian $P(E)$ or an additional line broadening mechanism.

Hexaquo Fe^{+2}

Mössbauer findings are compatible with the presence of hexaquo complexes of the ferrous ion in quenched aqueous solutions (43). The water molecules are weak-field ligands and form a rough octahedron about the iron ion resulting in a high-spin iron quintet. We have demonstrated earlier (10) that the EPR signals are due to resonance of a ground $|2^{\pm}\rangle$ doublet. The best EPR simulations use $D = -8$ K, $E = -2.05$ K and indicate a large width in the distribution of Δ_2-values, which hardly affects the interpretation of the magnetization data, however. The parameters deduced from the latter, $D = \pm 13$ K, $E/D \approx 0.3$ (10) do not match the EPR data perfectly, but it is difficult to deduce the correct parameters from EPR data that account for only ~5% of the spins. In addition, the distribution $P(E)$ may be skewed, or otherwise more complicated thus invalidating the assumption of a Gaussian distribution. The position of the resonance is dependent on D through the second order spin-orbit coupling corrections to the g values, Eq. 2 of reference 10. However, the dependence of the zero-field splitting on D presents an added complication and, in general, an independent determination of D is difficult from simulations alone.

The problem of deducing correct D and E values may be overshadowed by a more important question. Are large negative D-values physically meaningful? According to standard models (44), negative D-values imply low-lying, excited orbital states which may invalidate the spin Hamiltonian of Eq. 3. Clear evidence of a temperature-dependent quadrupole splitting in Mössbauer spectra exists in many ferrous complexes, suggesting an excited orbital level at ~300 K. For hexaquo Fe^{+2} the temperature dependence of the quadrupole splitting is relatively weak, however, and Eq. 3 should be valid over the limited temperature range of the EPR studies.

It is important to note that the best fit to the magnetic susceptibility data suggests $\Delta_2 \approx 3$ cm^{-1}, a value that is a factor of 10 larger than the energy of an X band spectrometer, yet EPR spectra are observable. Hexaquo Fe^{+2} is not an isolated case: FeEDTA and preliminary results from several other complexes have magnetization or Mössbauer data which suggest no X band EPR resonance, yet integer-spin signals have been observed. Thus,

Mössbauer or magnetization data should not deter one from trying EPR experiments.

The use of hexaquo Fe^{+2} as a quantitation standard is not recommended for several reasons. (*a*) The fraction of total spins observed is small and difficult to determine accurately. At sufficiently high microwave frequency, on the other hand, all spins satisfy the condition $\Delta_2 < h\nu$ and are thus observable. (*b*) Mössbauer experiments have shown that the ferrous ions are trapped in an unstable ice lattice when quenched in liquid nitrogen (43). If after quenching, the sample is warmed to 190 K, the ice lattice undergoes a nonreversible transformation (anneal) to a stable lattice. We have observed temperature hysteresis effects with EPR as well. (*c*) Subtle variations in intensity and lineshape, due to solvent and counter ion effects, suggest problems with reproducibility.

Iron (II) ethylenediaminetetraacetate (FeEDTA)

Sample heterogeneity precludes a definitive interpretation of the EPR data, but Fe^{+2} EDTA is of interest because of the persistence of its EPR signal up to 80 K, a feature not seen in any of the other integer-spin systems. According to the Mössbauer analysis summarized in Table 2, the FeEDTA sample contains two distinct Fe^{+2} species with different quadrupole splittings and possibly different zero-field splittings. It is not clear if the EPR signal arises from both species or from one only. The magnetization data of Fig. 8 yield an average value of the zero-field parameters, $D = \pm 13$ K, $E/D = 1/3$. The EPR simulations of Fig. 7 are obtained with $D = -13$ K, $E = -1.5$ K, $\sigma_E = 0.15$ K, but they do not match the data satisfactorily. Moreover, the temperature dependence of the EPR signal, Fig. 9, suggests a more negative value, $D \leq -16$ K. In summary, our model does not allow us to find a definitive parameter set, most likely because the sample contains two different Fe^{+2} species.

The FeEDTA EPR signal is observable at a significantly higher temperature than that of all other complexes in this study. At low temperature, $T = 4$ K, the signal saturates with relatively low microwave power. These observations suggest that the FeEDTA complex has a relatively slow relaxation rate. As the microwave power is increased, the behavior of the spectral lineshape is markedly field dependent and analogous to that shown in Fig. 14. The low-field edge near $B = 0$ saturates most easily. At higher microwave frequencies the absorption shifts away from $B = 0$ and low field saturation may not be as much a concern; this remains to be seen. Hagen (2) has suggested that lineshape changes like that of Fig. 14 are due to burn-out of spin-packets having low resonance field. However, the canonical relaxation mechanism, ligand-field modulation (20), has not yet been shown to predict easy saturation at low fields.

Model hemes

The EPR signal of the model heme complex Fe(II) 2-methylimidazole mesotetraphenylporphyrin (FeTPP) is remarkably similar to the signals of hexaquo Fe^{+2}, not only in shape but also in microwave power and temperature dependence. The simulations predict an EPR observable fraction of only ~5%, so it remains to be seen if analysis of data from such a small fraction is compatible with data taken at higher microwave frequency. High-field Mössbauer experiments on the same complex have been interpreted in terms of temperature-dependent quadrupole splitting and zero-field parameters (45), suggesting that the spin Hamiltonian, Eq. 3, is invalid.

No EPR signals were observed from the FeTPP(CO) model complexes under continuous illumination. Two possible explanations for the lack of a signal are: (*a*) the recombination of CO to iron is fast (70% of the photolyzed molecules rebind in 10^{-4} s [39]) and the equilibrium concentration of $S = 2$ centers is too small to be detected; (*b*) the zero-field splitting of the photodissociated compound does not satisfy the inequality, $\Delta_k > h\nu$, and thus no EPR signal is detectable. Although no EPR signals were found, this model complex serves as a control for the CO myoglobin experiments in the next section.

Myoglobin (Mb)

The myoglobin signals are similar to those of the hexaquo Fe^{+2} and the FeTPP model, but the trough of $d\chi''/dB$ is significantly different. Moreover, the temperature dependence of the Mb spectra is that of an excited doublet (10), but if the spin Hamiltonian, Eq. 3, is valid, thermal population alone cannot explain the temperature dependence of the EPR signal intensity. Indeed, with the parameters used to simulate the signal, it is surprising that any signal is observed at low temperature as the population of an excited doublet is quite small at $T = 4$ K. Most likely Eq. 3 is inadequate for Mb, a conclusion that follows from other lines of evidence to be summarized below. In view of this conclusion, we do not see a method of spin quantitation for Mb.

EPR signals from Hb have been observed at microwave frequencies up to 300 GHz (46). The temperature dependence of the Hb signal is similar to our findings for Mb, but only three temperature points are available from the Hb experiments. As mentioned in Results, we observed no integer-spin EPR signals from the photodissociated Hb*(CO) complex. The experiments were carried out

under conditions identical to the Mb*(CO) measurements.

For the EPR simulation of Mb, the center of the distribution in zero-field parameters was chosen to be consistent with the magnetic susceptibility data (40) with the width σ_D adjusted to allow for consistency with far-infrared data (22). Interestingly, the ratio $\sigma_D/D \approx 0.2$ for ferrous Mb is found to be approximately equal to that of ferric Mb recently noted by Levin and Brill (36), suggesting that comparable, large heterogeneity exists in both oxidation states.

The validity of the spin Hamiltonian, Eq. 3, for Mb and Hb has been questioned (22, 28, 46, 47, 48) because of possible nearby states which originate outside of the ^5D term. A number of theoretical models have been proposed to explain the magnetic data of Mb and Hb. None of the models to date consistently explains all of the experimental data. The more important recent experimental findings are:

(*a*) According to magnetic susceptibility measurements on Mb (49), Mb*(CO) (40), and Hb (50, 51), the magnetic moment is close to the free spin value, $\mu_{eff} = 4.9\mu_b$, for $T > 20$ K. Consequently, either the orbital angular momentum is quenched, $\langle \mathbf{L} \rangle = 0$, or else the wavefunction contains admixtures of states with $S < 2$.

(*b*) Mössbauer measurements over the temperature range 10–240 K (45, 48, 52) show a temperature-dependent quadrupole splitting, ΔE_Q, suggesting the population of a nearby excited orbital state.

(*c*) The principal component of the electric field gradient tensor is negative, $V_{ZZ} < 0$, and none of the tensor's principal axes are aligned near the heme normal (45, 47, 53).

(*d*) Far-infrared magnetic resonance measurements find a magnetic doublet split by ~6 K. No other transitions are observed within 20 K, and the one doublet accounts for the low-temperature DC magnetic susceptibility (22).

(*e*) High-spin $S = 2$ EPR signals are observed in the temperature range 2–30 K and frequency range 9–300 GHz (10, 46) with a temperature dependence that is inconsistent with the spin Hamiltonian of a quintet.

Findings (*a*) and (*b*) seem to be contradictory as the nearby orbital states necessary for a temperature-dependent ΔE_Q will admix through the spin-orbit interaction and tend to unquench $\langle \mathbf{L} \rangle$. The magnetic susceptibility data of Nakano et al. (49) and Roder et al. (40) can be fitted well with a $S = 2$ spin Hamiltonian and $D \approx 7$ K, but such a fit contradicts findings (*d*) and (*e*). Several models (48, 52) that proposed more complicated electronic energy level schemes contain assumptions at variance with findings (*a*) and (*c*). Most recently Kent et al. (47) considered several electronic schemes for Mb based on the ^5D term of Fe^{+2}. They found that none of the schemes was compatible with all the experimental facts and concluded that the ^5D term alone is inadequate and that other terms must be admixed. In view of findings (*d*) and (*e*), it appears that electronic models cannot ignore sample heterogeneity of the type we attempt to describe by distributions of the zero-field parameters.

Cytochrome *c* oxidase

The "$g = 12$" EPR signal in oxidized C*c*O has long been thought to arise from an integer-spin system (54), and several attempts to analyze this signal have appeared in the literature (2, 7, 25). Here we add a few new observations, we note that our model fails to simulate the signal quantitatively, and we speculate about possible reasons for this failure.

C*c*O is the terminal oxidase of the respiratory chain in mitochondria; it is known to contain two hemes, heme *a* and heme a_3, and two copper atoms, Cu_A and Cu_B, in an active site whose detailed structure has not been resolved yet. Most efforts to arrive at reproducible and homogeneous preparations of C*c*O have been made with beef heart (55, 56) but yeast C*c*O has also been characterized in detail (9, 17). The "$g = 12$" state of the oxidized enzyme has low activity (55) and is possibly an artifact (57); it is of interest nevertheless, because it contains a spin-coupled pair of high-spin heme a_3, $S_{Fe} = 5/2$, and Cu_B^{+2}, with an effective spin of $S = 2$. The spin coupling implies that the two metals are close together, presumably bridged by a chloride ion (57), and one can speculate that the active form of the enzyme has a closely related structure.

As is evident from Fig. 12 *a*, C*c*O from yeast shows two distinct "$g = 12$" type EPR signals, and comparison with the signal of C*c*O from beef heart in Fig. 12 *b* suggests that the latter also consists of two superimposed signals, albeit of different intensities. Assuming that the spins of heme a_3 and of Cu_B are strongly coupled to an effective spin of $S = 2$, the spin Hamiltonian, Eq. 3, should apply to the coupled system. As a consequence, the "$g = 12$" signal should be described by our lineshape model that derives from Eq. 3. So far all attempts to simulate the "$g = 12$" spectra have failed, however assuming either $k = 1$ or $k = 2$ in Eq. 5. The problem conceivably arises from the fact that the spectra are superpositions of two signals that cannot be separated yet. We have also attempted to simulate data from Hagen's work (2). Hagen's spectrum using $\mathbf{B}_1 \parallel \mathbf{B}$ shows one component only and simulations of this spectrum do give a closer, although not exact, fit with our model. However, no spectra using $\mathbf{B}_1 \perp \mathbf{B}$ were presented to allow for a check of Eq. 13.

Another explanation is suggested by the observation that the "$g = 12$" signal resembles the spectrum of $Mb^*(O_2)$, as illustrated in Fig. 15, a spectrum that our lineshape model does not reproduce either. In the case of $Mb^*(O_2)$ it is pretty obvious that the spin Hamiltonian, Eq. 3, is not adequate. According to the EPR spectra the electronic state of the heme iron in Mb*(CO) is indistinguishable from that in Mb, at least on the time scale (10^3 s) of the experiment, and one would expect the same state of the iron in $Mb^*(O_2)$ as well. The pronounced difference in the EPR spectra of $Mb^*(O_2)$ and Mb*(CO), respectively, is most likely due to the presence of the spin $S = 1$ of the O_2, which interacts magnetically with the spin $S = 2$ of the iron. The Hamiltonian of the $Mb^*(O_2)$ system is therefore quite different from Eq. 3, and it is no wonder that the model derived from the latter does not describe the EPR of $Mb^*(O_2)$. Extending the argument to C*c*O, we propose that C*c*O does not satisfy the assumptions of our model. The Fe^{+3}-Cu^{+2} system may either have a larger number of degrees of freedom than Eq. 3, e.g., if the exchange interaction between the two spins is not very strong or terms in S^4 are not negligible (25, 58), or else the assumption is incorrect that the transition matrix element is given entirely by $\langle k^{\pm}|S_z|k^{\mp}\rangle$, e.g., in Eq. 7. A hint of the last possibility comes from our attempts to simulate the spectra taken with $\mathbf{B}_1 \parallel \mathbf{B}$ and $\mathbf{B}_1 \perp \mathbf{B}$ in Figs. 12, *b* and *c*, as it proved impossible to reproduce the intensity ratios assuming the validity of Eq. 13.

In summary, a quantitative interpretation of the "$g = 12$" signal of C*c*O is still lacking. The simple model of a spin quintet with transitions within the $|k^{\pm}\rangle$ doublets is inadequate, and a more systematic study appears necessary using EPR at different frequencies in combination with magnetization and Mössbauer measurements.

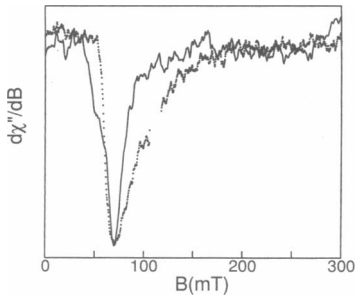

FIGURE 15 Frozen solution EPR spectra of cytochrome oxidase from bovine heart (_) and photodissociated oxymyoglobin, $Mb^*(O_2)$ (. . .) at $T = 4$ K using $\mathbf{B}_1 \parallel \mathbf{B}$. The oxidase spectrum is reproduced from Fig. 12 *b* and $Mb^*(O_2)$ spectrum is reproduced from Fig. 6 *a* of reference 10. Comparison of signals using $\mathbf{B}_1 \perp \mathbf{B}$ cannot yet be made, as such a signal has not been observed from $Mb^*(O_2)$ due to signals from ferric impurities which mask the region of interest.

Azide complex of hemerythrin

Another integer-spin EPR signal has been reported by Reem and Solomon (3, 24) in deoxyhemerythrin azide. Hemerythrin is the oxygen carrier protein of marine worms and contains two high-spin iron atoms in a binuclear site with three bridging ligands, a μ-hydroxo group (3), a glutamate and an aspartate. In deoxyhemerythrin both irons are ferrous; one is five-coordinate and can bind O_2 or anions like azide. Fig. 13 shows the EPR signals of hemerythrin azide for the two field orientations $\mathbf{B}_1 \parallel \mathbf{B}$ and $\mathbf{B}_1 \perp \mathbf{B}$; it has all the characteristic features of integer-spin EPR, i.e., $d\chi''/dB$ is negative throughout and reaches its minimum at rather low fields, and the signal is considerably stronger for $\mathbf{B}_1 \parallel \mathbf{B}$ than $\mathbf{B}_1 \perp \mathbf{B}$. The last feature suggests that the EPR transitions arise from the matrix element $\langle k^{\pm}|S_z|k^{\mp}\rangle$ rather than from $\langle k^{\pm}|S_{\pm}|k^{\mp}\rangle$. Fig. 14 illustrates the peculiar saturation behavior of the EPR signal of hemerythrin azide, which is typical of several integer-spin systems. The low-field part of $d\chi''/dB$ saturates more readily than the rest of the spectrum for reasons that are presently not understood. Not surprisingly, our lineshape model for a $S = 2$ Hamiltonian, Eq. 3, is unable to reproduce the observed spectra. Even if the exchange interaction, $J\mathbf{S}_1 \cdot \mathbf{S}_2$, between two ferrous ions should be negligible, the dipole–dipole interaction may be strong compared with the Zeeman interaction at the fields of interest, thus a more complicated Hamiltonian than Eq. 3 must be used to describe the system.

Reem and Solomon suggest a ferromagnetic coupling between the two Fe^{+2} ions (3, 24), and they assign the EPR signal to transitions in a spin-admixed ground doublet $|\pm 4\rangle$. Their interpretation of the EPR data is weak, however, on several accounts. (*a*) It is unjustified to base a spin assignment of $S = 4$ on the effective *g*-value, $g_{\text{eff}} \approx 16$, of the minimum in $d\chi''/dB$ as several other integer-spin complexes with $S \neq 4$ show EPR signals peaking near $g_{\text{eff}} = 16$, for instance FeEDTA, ferredoxin II (5, 6), and aconitase (Hendrich, M., unpublished result). Before an assignment can be considered definitive it should at least lead to a quantitative simulation of the EPR spectra. (*b*) The increased intensity of the $\mathbf{B}_1 \parallel \mathbf{B}$ spectrum relative to the $\mathbf{B}_1 \perp \mathbf{B}$ spectrum, shown in Fig. 13, is a characteristic feature of EPR transitions mediated by the matrix elements $\langle k^{\pm}|S_z|k^{\mp}\rangle$ rather than $\langle k^{\pm}|S_{\pm}|k^{\mp}\rangle$. The statement that only $\delta m_s = \pm 1$ transitions are allowed in the normal microwave configuration, i.e., for $\mathbf{B}_1 \perp \mathbf{B}$ (24) is inappropriate in the present context since the dominant interaction for integer-spin systems of low symmetry is the zero-field splitting. The quantization axis *z* is therefore defined by the first term of Eq. 3, and the periodic perturbation, $\beta\mathbf{B}_1 \cdot \mathbf{g} \cdot \mathbf{S}$, has finite S_z matrix elements for all molecules whose *z*-axis is not perpendicu-

lar to **B**. We conclude that the origin of the EPR signal in hemerythrin azide is not fully understood and that more work is needed to arrive at a quantitative interpretation.

CONCLUSION

We have put forth a quantitative basis for the analysis of integer-spin EPR signals from metal centers with large zero-field splittings. The measurements and analyses on a variety of iron(II) compounds have lead to new insights on protein states that are generally thought not to be accessible with EPR.

We find sizable spreads in zero-field splitting parameters, and such spreads cannot be overlooked if the interpretation of magnetic data from several techniques is combined for protein characterization. This work clearly demonstrates the need for data at higher microwave frequencies. Higher frequency data will most certainly allow a better analysis of spectra, increase quantitation accuracy, reduce computer simulation time, and improve the chances of finding new signals from metal centers with even larger zero-field splittings.

We are indebted to Prof. Donald Kurtz for the hemerythrin sample, Dr. Hsin Wang for the cytochrome oxidase samples, Prof. Christopher Reed for the model heme complex, and Dr. Gerald Wagner for helpful suggestions concerning biochemical technique. The Q band spectra were taken at the Regional ESR Center, Milwaukee, WI. Dr. Hendrich would also like to thank Prof. Eckard Münck for his support and discussions.

This work was funded in part by National Institutes of Health grant GM16406.

Received for publication 23 February 1989 and in final form 22 May 1989.

REFERENCES

1. Hendrich, M. P., G. C. Wagner, and P. G. Debrunner. 1987. EPR spectra of quintet ferrous myoglobin and a model heme compound. *Bull. Am. Phys. Soc.* 32:479.
2. Hagen, W. R. 1982. EPR of non-Kramers doublets in biological systems. Characterization of an S = 2 system in oxidized cytochrome *c* oxidase. *Biochim. Biophys. Acta.* 708:82–98.
3. Reem, R. C., and E. I. Solomon. 1984. MCD-EPR studies of deoxy[FeII,FeII]hemerythrin: probes of endogenous bridging ligands and exogenous ligand binding. *J. Am. Chem. Soc.* 106:8323–8325.
4. Fox, B. G., K. K. Surerus, E. Münck, and J. D. Lipscomb. 1988. Evidence for a μ-oxo bridged binuclear iron cluster in the hydroxylase component of methane monooxygenase: Mössbauer and EPR studies. *J. Biol. Chem.* 263:10553–10556.
5. Papaefthymiou, V., J. J. Girerd, I. Moura, J. J. G. Moura, and E. Münck. 1987. Mössbauer study of *D. gigas* ferredoxin II and spin-coupling model for the Fe_3S_4 cluster with valence delocalization. *J. Am. Chem. Soc.* 109:4703–4710.
6. Hagen, W. R., W. R. Dunham, M. K. Johnson, and J. A. Fee. 1985. Quarter field resonance and integer-spin/half-spin interaction in the EPR of *Thermus thermophilus* ferredoxin. Possible new fingerprints for three iron clusters. *Biochim. Biophys. Acta.* 828:369–374.
7. Dunham, W. R., R. H. Sands, R. W. Shaw, and H. Beinert. 1983. Multiple frequency EPR study on three forms of oxidized cytochrome *c* oxidase. *Biochim. Biophys. Acta.* 748:73–85.
8. Brudvig, G. W., T. H. Stevens, R. H. Morse, and S. I. Chan. 1981. Conformations of oxidized cytochrome *c* oxidase. *Biochemistry.* 20:3912–3921.
9. Wang, H. 1987. Mössbauer and spectroscopic studies of yeast cytochrome oxidase. Ph.D. thesis. California Institute of Technology, Pasadena, CA.
10. Hendrich, M. P., and P. G. Debrunner. 1988. EPR spectra of quintet ferrous myoglobin and a model heme compound. *J. Magn. Res.* 78:133–141.
11. Wasserman, E., L. C. Snyder, and W. A. Yager. 1964. ESR of the triplet states of randomly oriented molecules. *J. Chem. Phys.* 41:1763–1772.
12. Tinkham, M. 1956. Paramagnetic resonance in dilute iron group fluorides. I. Fluorine hyperfine structure. *Proc. R. Soc. Lond. A.* 236:535–563.
13. Rubins, R. S. 1962. On the paramagnetic resonance spectrum of divalent iron in zinc fluosilicate. *Proc. Phys. Soc. (Lond.).* 80:244–247.
14. Rubins, R. S., and T. D. Black. 1981. Electron paramagnetic resonance in ferrous fluosilicate near 10 K. *Chem. Phys. Lett.* 81:450–452.
15. Collman, J. P., and C. A. Reed. 1973. Syntheses of ferrous-porphyrin complexes. A hypothetical model for deoxymyoglobin. *J. Am. Chem. Soc.* 95:2048–2049.
16. Wagner, G. C., and R. J. Kassner. 1975. Spectroscopic properties of ferrous heme complexes of sterically hindered ligands. *Biochim. Biophys. Acta.* 392:319–327.
17. Stevens, T. H., C. T. Martin, H. Wang, G. W. Brudvig, C. P. Scholes, and S. I. Chan. 1982. The nature of Cu_A in cytochrome *c* oxidase. *J. Biol. Chem.* 257:12106–12113.
18. Maier, L. C., Jr. and J. C. Slater. 1952. Field strength measurements in resonant cavities. *J. Appl. Phys.* 23:68–77.

18a. Poole, C. P., Jr. 1983. Electron Spin Resonance. 2nd ed. John Wiley & Sons, New York. 171.

19. Brackett, G. C., P. L. Richards, and W. S. Caughey. 1971. Far-infrared magnetic resonance in Fe(III) and Mn(III) porphyrins, myoglobin, hemoglobin, ferrichrome A, and Fe(III) dithiocarbamates. *J. Chem. Phys.* 54:4383–4401.
20. Abragam, A., and B. Bleaney. 1970. Electron Paramagnetic Resonance of Transition Ions. Clarendon Press, Oxford.
21. Champion, P. M., and A. J. Sievers. 1977. Far infrared magnetic resonance in $FeSiF_6 \cdot 6H2O$ and $Fe(SPh)_4^{-2}$. *J. Chem. Phys.* 66:1819–1825.
22. Champion, P. M., and A. J. Sievers. 1980. Far infrared magnetic resonance of deoxyhemoglobin and deoxymyoglobin. *J. Chem. Phys.* 72:1569–1582.
23. Rubins, R. S., and H. R. Fetterman. 1979. Electron paramagnetic resonance in ferrous fluosilicate at submillimeter wavelengths. *J. Chem. Phys.* 71:5163–5166.
24. Reem, R. C., and E. I. Solomon. 1987. Spectroscopic studies of the

binuclear ferrous active site of deoxyhemerythrin: coordination number and probable bridging ligands for the native and ligand bound forms. *J. Am. Chem. Soc.* 109:1216–1226.

25. Brudvig, G. W., R. H. Morse, and S. I. Chan. 1986. A comparison of an exchanged-coupled Fe(III)-Cu(II) model with a Fe(IV) model for the O_2 binding site in oxidized cytochrome *c* oxidase via EPR spectral simulations. *J. Magn. Res.* 67:189–201.
26. Baym, G. 1969. Lectures on Quantum Mechanics. Benjamin/ Cummings, Reading, UK. 251.
27. Aasa, R., and T. Vänngård. 1975. EPR signal intensity and powder shapes: a reexamination. *J. Magn. Res.* 19:308–315.
28. Lumpkin, O., and W. T. Dixon. 1978. Low temperature proton NMR in deoxymyoglobin and a new model for the low-lying Fe^{+2} states. *J. Chem. Phys.* 68:3485–3496.
29. Winkler, H., C. Schulz, and P. G. Debrunner. 1979. Spin fluctuation rates from Mössbauer spectra of high-spin ferrous rubredoxin. *Phys. Lett.* 69A:360–363.
30. Schulz, C. E., P. Nyman, and P. G. Debrunner. 1987. Spin fluctuations of paramagnetic iron centers in proteins and model complexes: Mössbauer and EPR results. *J. Chem. Phys.* 87:5077–5091.
31. Hagen, W. R., D. O. Hearshen, L. J. Harding, and W. R. Dunham. 1985. Quantitative numerical analysis of g strain in the EPR of distributed systems and its importance for multicenter metalloproteins. *J. Magn. Res.* 61:233–244.
32. Bleaney, B., and H. E. D. Scovil. 1952. Paramagnetic resonance in praseodymium ethylsulphate. *Philos. Mag.* 43:999–1000.
33. Baker, J. M., and B. Bleaney. 1958. Paramagnetic resonance in some lanthanon ethyl sulphates. *Proc. R. Soc. (Lond.).* A245:156–174.
34. Griffith, J. S. 1963. Spin hamiltonian for even-electron systems having even multiplicity. *Phys. Rev.* 132:316–319.
35. Levin, P. D. 1984. EPR power saturation recovery in high-spin ferric heme systems: measuring and modeling the effects of energy level distributions. Ph.D. thesis. University of Virginia, Charlottesville, VA.
36. Levin, P. D., and A. S. Brill. 1988. Analysis of EPR pulse saturation recovery kinetics of myoglobin solutions. *J. Phys. Chem.* 92:5103–5113.
37. Schulz, C. E. 1979. Mössbauer and EPR studies of iron-containing proteins. Ph.D. thesis. University of Illinois, Urbana, IL.
38. Hamilton, W. C. 1962. Bond distances and thermal motion in ferrous fluosilicate hexahydrate: a neutron diffraction study. *Acta Crystallogr.* 15:353–360.
39. Chan, S. S. 1977. Dynamics of carbon monoxide binding to protoheme and heme *c* octapeptide. Ph.D. thesis. University of Illinois, Urbana, IL.
40. Roder, H., J. Berendzen, S. F. Bowne, H. Frauenfelder, T. B. Sauke, E. Shyamsunder, and M. B. Weissman. 1984. Comparison of the magnetic properties of deoxy- and photodissociated myoglobin. *Proc. Natl. Acad. Sci. USA.* 81:2359–2363.
41. Ansari, A., J. Berendzen, D. Braunstein, B. R. Cowen, H. Frauenfelder, M. K. Hong, I. E. T. Iben, J. B. Johnson, P. Ormos, T. B. Sauke, R. Scholl, A. Schulte, P. J. Steinbach, J. Vittitow, and R. D. Young. 1987. Rebinding and relaxation in the myoglobin pocket. *Biophys. Chem.* 26:337–355.
42. LoBrutto, R., Y. Wei, S. Yoshida, H. L. van Camp, C. P. Scholes, and T. E. King. 1984. Electron paramagnetic resonance- (EPR-) resolved kinetics of cryogenic nitric oxide recombination to cytochrome *c* oxidase and myoglobin. *Biophys. J.* 45:473–479.
43. Nozik, A. J., and M. Kaplan. 1967. Mössbauer resonance studies of ferrous ions in ice. *J. Chem. Phys.* 47:2960–2976.
44. Ingalls, R. 1964. Electric-field gradient tensor in ferrous compounds. *Phys. Rev.* 133:A787–A795.
45. Kent, T. A., K. Spartalian, G. Lang, T. Yonetani, C. A. Reed, and J. P. Collman. 1979. High magnetic field Mössbauer studies of deoxymyoglobin, deoxyhemoglobin and synthetic analogues. *Biochim. Biophys. Acta.* 580:245–258.
46. Alpert, Y. 1975. Contribution à la connaissance des propriétés électroniques du fer dans L'hémoglobine: données spectroscopiques et magnétiques. Ph.D. thesis. University of Paris.
47. Kent, T. A., K. Spartalian, and G. Lang. 1979. High magnetic field Mössbauer studies of deoxymyoglobin, deoxyhemoglobin, and synthetic analogues: theoretical interpretation. *J. Chem. Phys.* 71:4899–4908.
48. Huynh, B. H., G. C. Papaefthymiou, C. S. Yen, J. L. Groves, and C. S. Wu. 1974. Electronic structure of Fe^{+2} in normal human hemoglobin and its isolated subunits. *J. Chem. Phys.* 61:3750–3758.
49. Nakano, N., J. Otsuka, and A. Tasaki. 1971. Fine structure of iron ion in deoxymyoglobin and deoxyhemoglobin. *Biochim. Biophys. Acta.* 236:222–233.
50. Nakano, N., J. Otsuka, and A. Tasaki. 1972. Paramagnetic anisotropy measurements on a single crystal of deoxyhemoglobin. *Biochim. Biophys. Acta.* 278:355–371.
51. Alpert, Y., and R. Banerjee. 1975. Magnetic susceptibility measurements of deoxygenated hemoglobins and isolated chains. *Biochim. Biophys. Acta.* 405:144–154.
52. Eicher, H., D. Bade, and F. Parak. 1976. Theoretical determination of the electronic structure and spatial arrangement of ferrous ion in deoxygenated sperm whale myoglobin and human hemoglobin from Mössbauer experiments. *J. Chem. Phys.* 64:1446–1455.
53. Kent, T., K. Spartalian, G. Lang, and T. Yonetani. 1977. Mössbauer investigation of deoxymyoglobin in a high magnetic field: orientation of the electric field gradient and magnetic tensors. *Biochim. Biophys. Acta.* 490:331–340.
54. Van Gelder, B. F., and H. Beinert. 1969. Studies of the heme components of cytochrome *c* oxidase by EPR spectroscopy. *Biochim. Biophys. Acta.* 189:1–24.
55. Baker, G. M., M. Noguchi, and G. Palmer. 1987. The reaction of cytochrome oxidase with cyanide. *J. Biol. Chem.* 262:595–604.
56. Steffens, G. C. M., R. Biewald, and G. Buse. 1987. Cytochrome *c* oxidase is a three-copper, two-heme-A protein. *Eur. J. Biochem.* 164:295–300.
57. Scott, R. A., P. M. Li, and S. I. Chan. 1988. The binuclear site of cytochrome *c* oxidase. Structural evidence from iron absorption x-ray spectroscopy. *Ann. NY Acad. Sci.* 550:53–58.
58. Rudowicz, C. 1987. Concept of spin Hamiltonian, forms of zero field splitting and electronic Zeeman Hamiltonians and relations between parameters used in EPR. A critical review. *Magn. Res. Rev.* 13:1–89.